

# Characteristics and trends in various forms of the Palmer Drought Severity Index during 1900–2008

Aiguo Dai<sup>1</sup>

Received 21 December 2010; revised 17 March 2011; accepted 29 March 2011; published 29 June 2011.

[1] The Palmer Drought Severity Index (PDSI) has been widely used to study aridity changes in modern and past climates. Efforts to address its major problems have led to new variants of the PDSI, such as the self-calibrating PDSI (sc\_PDSI) and PDSI using improved formulations for potential evapotranspiration (PE), such as the Penman-Monteith equation (PE\_pm) instead of the Thornthwaite equation (PE\_th). Here I compare and evaluate four forms of the PDSI, namely, the PDSI with PE\_th (PDSI\_th) and PE\_pm (PDSI\_pm) and the sc\_PDSI with PE\_th (sc\_PDSI\_th) and PE\_pm (sc\_PDSI\_pm) calculated using available climate data from 1850 to 2008. Our results confirm previous findings that the choice of the PE only has small effects on both the PDSI and sc\_PDSI for the 20th century climate, and the self-calibration reduces the value range slightly and makes the sc\_PDSI more comparable spatially than the original PDSI. However, the histograms of the sc\_PDSI are still non-Gaussian at many locations, and all four forms of the PDSI show similar correlations with observed monthly soil moisture ( $r = 0.4\text{--}0.8$ ) in North America and Eurasia, with historical yearly streamflow data ( $r = 0.4\text{--}0.9$ ) over most of the world's largest river basins, and with GRACE (Gravity Recovery and Climate Experiment) satellite-observed water storage changes ( $r = 0.4\text{--}0.8$ ) over most land areas. All the four forms of the PDSI show widespread drying over Africa, East and South Asia, and other areas from 1950 to 2008, and most of this drying is due to recent warming. The global percentage of dry areas has increased by about 1.74% (of global land area) per decade from 1950 to 2008. The use of the Penman-Monteith PE and self-calibrating PDSI only slightly reduces the drying trend seen in the original PDSI. The percentages of dry and wet areas over the global land area and six select regions are anticorrelated ( $r = -0.5$  to  $-0.7$ ), but their long-term trends during the 20th century do not cancel each other, with the trend for the dry area often predominating over that for the wet area, resulting in upward trends during the 20th century for the areas under extreme (i.e., dry or wet) conditions for the global land as a whole (~1.27% per decade) and the United States, western Europe, Australia, Sahel, East Asia, and southern Africa. The recent drying trends are qualitatively consistent with other analyses and model predictions, which suggest more severe drying in the coming decades.

**Citation:** Dai, A. (2011), Characteristics and trends in various forms of the Palmer Drought Severity Index during 1900–2008, *J. Geophys. Res.*, 116, D12115, doi:10.1029/2010JD015541.

## 1. Introduction

[2] Drought is a recurring extreme climate event over land characterized by below-normal precipitation over a period of several months to several years or even a few decades. It is among the most damaging natural disasters, causing tens of billions of dollars in damage and affecting millions of people in the world each year [Wilhite, 2000]. To quantify drought and monitor its development, many drought indices have been developed and applied [Heim, 2000, 2002; Keyantash

and Dracup, 2002; Vicente-Serrano *et al.*, 2010a; Dai, 2011]. Among them, the Palmer Drought Severity Index (PDSI) is the most prominent index of meteorological drought used in the United States for drought monitoring and research [Heim, 2002]. The PDSI and its variants have been used to quantify long-term changes in aridity over land in the 20th [Dai *et al.*, 1998, 2004; van der Schrier *et al.*, 2006a, 2006b, 2007; Dai, 2011] and 21st [Burke *et al.*, 2006; Burke and Brown, 2008; Dai, 2011] century. The PDSI has also been widely used in tree ring-based reconstructions of past droughts in North America and other regions [e.g., Cook *et al.*, 2004, 2007].

[3] The PDSI was originally developed by Palmer [1965] with the intent to measure the cumulative departure in sur-

<sup>1</sup>National Center for Atmospheric Research, Boulder, Colorado, USA.

face water balance. It incorporates antecedent and current moisture supply (precipitation,  $P$ ) and demand (potential evapotranspiration,  $PE$ ) into a hydrological accounting system, which includes a two-layer bucket-type model for soil moisture calculations. The PDSI is a standardized measure, ranging from about  $-10$  (dry) to  $+10$  (wet) with values below  $-3$  representing severe to extreme drought. The standardization used by Palmer was based on limited data from the central United States and tends to yield more severe PDSI in the Great Plains than other U.S. regions [Guttman *et al.*, 1992]. To improve the spatial comparability, Wells *et al.* [2004] proposed a self-calibrating PDSI ( $sc\_PDSI$ ) by calibrating the PDSI using local conditions, instead of using the (fixed) coefficients used by Palmer [1965] based on data from the central United States. The  $sc\_PDSI$  performed better than the original PDSI during the 20th century over Europe and North America [van der Schrier *et al.*, 2006a, 2006b, 2007].

[4] Another major complaint about the PDSI is that the  $PE$  calculated using the Thornthwaite equation [Thornthwaite, 1948] in the original Palmer model could lead to errors in energy-limited regions [Hobbins *et al.*, 2008], as the Thornthwaite  $PE$  ( $PE_{th}$ ) is based only on temperature, latitude, and month. This error can be minimized, however, by using the more sophisticated Penman-Monteith equation (referred to as  $PE_{pm}$  [Burke *et al.*, 2006]), which accounts for the effects of radiation, humidity, and wind speed and works best over Australia in a comparison of various  $PE$  formulations by Donohue *et al.* [2010]. Palmer [1965] chose the  $PE_{th}$  mainly based on practical considerations as data for computing  $PE_{pm}$  and other types of  $PE$  might be unavailable. This is especially true for global analyses.

[5] The PDSI is also imprecise in its treatment of all precipitation as immediately available rainfall (i.e., no delayed runoff from melting snow), its lack of impact of vegetation or frozen soils on evaporation, and some other processes [Alley, 1984]. Despite all these caveats, Dai *et al.* [2004] showed that the PDSI values are significantly correlated with measured soil moisture content in the warm season and streamflow over many regions over the world and thus can be used as a measure of drought, especially over the low and middle latitudes. This is largely due to the fact that the normalization in the Palmer model minimizes the errors associated with many of the assumptions made by Palmer [1965] and that actual evaporation is often determined, to a large degree, by the availability of soil moisture (and thus affected by precipitation), not by  $PE$ , over many land areas [Willmott *et al.*, 1985]. Also, using annual values should minimize the seasonal effect of snowfall on the surface water balance.

[6] Recently, the PDSI was criticized for its inability to depict droughts on time scales shorter than 12 months when monthly PDSI values were used [Vicente-Serrano *et al.*, 2010b]. This is not unexpected as the PDSI was designed to be strongly autocorrelated in order to account for the impact of land memory on drought conditions. However, the Palmer model also computes the unsmoothed  $Z$  index, which can be used to track short-term agricultural drought, since it responds quickly to changes in soil moisture, as pointed out by Karl [1986]. For quantifying long-term changes in aridity and droughts, the relatively long intrinsic time scale of monthly PDSI should not be a problem.

[7] On the positive side, the PDSI is based on a physical water-balance model, uses both precipitation and surface air

temperature (and other variables when  $PE_{pm}$  is used) as input, and takes the precedent condition into account, in contrast to most other drought indices that are based purely on past statistics of certain climate variables, which often include precipitation alone [Keyantash and Dracup, 2002; Dai, 2011]. The standardized precipitation evapotranspiration index recently developed by Vicente-Serrano *et al.* [2010a] considers the difference between precipitation and potential evapotranspiration. However, as shown below, it is the actual evapotranspiration ( $E$ ), not the  $PE$ , that affects the surface water balance and thus the drought conditions. And because the  $PE$  and  $E$  are often decoupled or even anticorrelated over many water-limited land areas [Brutsaert, 2006] where drought studies are most relevant, a physical model is necessary to calculate current moisture condition near the surface, from which (and the precedent states) a good drought index may be derived.

[8] From this perspective, the PDSI and  $sc\_PDSI$  may be considered superior to other statistically based drought indices. This is because the PDSI and  $sc\_PDSI$  can account for the basic effect of global warming through Palmer's water balance model on droughts and wet spells. The effect of global warming may have already occurred during the 20th century [Dai *et al.*, 2004; van der Schrier *et al.*, 2006a, 2006b; Dai, 2011] and may increase substantially in the 21st century [Burke and Brown, 2008; Dai, 2011]. The effect of surface temperature, which accounts for 10%–30% of PDSI's variance during the 20th century, comes mainly through potential evapotranspiration. As precipitation and surface air temperature are the only two climate variables with long historical records, the PDSI makes full use of these data and can be readily calculated for the last hundred years or so for most land areas [Dai *et al.*, 2004; Dai, 2011].

[9] Despite its wide applications, the characteristics and performance of the original and modified versions of the PDSI (i.e., PDSI and  $sc\_PDSI$  with  $PE_{th}$  versus with  $PE_{pm}$ ) have not been well examined over the global land. In particular, the impact on long-term trends in the PDSI during the 20th century by the above-mentioned modifications has not been well studied, although some comparisons between the PDSI and  $sc\_PDSI$  and the impact of  $PE_{pm}$  on the resulting PDSI have been discussed [e.g., Burke *et al.*, 2006; van der Schrier *et al.*, 2006a, 2006b]. In particular, van der Schrier *et al.* [2011] examined the impact of the  $PE_{th}$  and  $PE_{pm}$  on the  $sc\_PDSI$  and found that the choice of the  $PE$  has a small effect because of the insensitivity of the required precipitation (see equation (2) below) to the  $PE$  in the Palmer model. The goal of this study is to compare the characteristics of the various forms of the PDSI, evaluate their performance as a drought index using available historical records of soil moisture and streamflow, compare trends in the different forms of the PDSI during the 20th century, and investigate the drying effect of recent warming. The results should help us better understand the various Palmer drought indices and the aridity changes in the 20th and 21st centuries.

[10] This study follows the general approach and updates the analysis of Dai *et al.* [2004], who evaluated the performance of the traditional PDSI and examined its long-term changes. As a result, some of the figures presented below look similar to those in the work of Dai *et al.* [2004]. However, besides including new data for 2003–2008, this study presents new results on the characteristics of the various forms of

**Table 1.** Data Sets Used in This Study<sup>a</sup>

Variables	Type and Coverage	Resolution	Period	Source and Reference
Precipitation	Rain gauge, land	$2.5^\circ \times 2.5^\circ$	1850–2008	<i>Dai et al. [1997], Chen et al. [2002], Huffman et al. [2009]</i>
Surface air temperature	Surface observations, land	$2.5^\circ \times 2.5^\circ$	1850–2008	CRUTEM3; <i>Brohan et al. [2006]</i>
Surface wind speed, humidity, and air pressure	Reanalysis data	$2.5^\circ \times 2.5^\circ$	1948–2008; climatology for other years	<i>Kalnay et al. [1996], Qian et al. [2006]</i>
Cloud cover	Surface observations, land	$2.5^\circ \times 2.5^\circ$	1948–2004; climatology for other years	<i>Dai et al. [2006], Qian et al. [2006]</i>
Net surface solar radiation	Observations and CLM3- based estimates	$2.5^\circ \times 2.5^\circ$	1948–2004; climatology for other years	<i>Qian et al. [2006]</i>
Streamflow	Gauge, 230 rivers	Yearly	1948–2004	NCAR; <i>Dai et al. [2009]</i>
Soil moisture	Station observations	Monthly	10–21 years	<i>Robock et al. [2000]</i>
	Illinois	19 stations	1981–2001	<i>Hollinger and Isard [1994]</i>
	China	43 stations	1981–1991	<i>Robock et al. [2000]</i>
	Mongolia	42 stations	1978–1993	<i>Robock et al. [2000]</i>
	Former USSR	50 stations	1972–1985	<i>Vinnikov and Yeserkepova [1991]</i>
Liquid water equivalent thickness	GRACE satellite observations, global land	$1^\circ \times 1^\circ$	Apr 2002 to Dec 2010	<i>Swenson and Wahr [2006];</i> <a href="http://grace.jpl.nasa.gov/">http://grace.jpl.nasa.gov/</a>
Soil water-holding capacity	Derived	$1^\circ \times 1^\circ$	Climatology	<i>Webb et al. [1993]</i>

<sup>a</sup>All are monthly except stated otherwise.

the PDSI, the performance of and changes in the other forms of the PDSI, and comparisons with Gravity Recovery and Climate Experiment (GRACE) satellite data and with land-model simulated soil moisture changes. Furthermore, the forcing data for precipitation of recent decades in this study are from a source different from that used by *Dai et al. [2004]*.

[11] Below, I first describe the data sets used in this study in section 2, followed by a description of the relevant aspects of the various forms of the PDSI and their characteristics in section 3. Section 4 presents a comparison with observed soil moisture and streamflow, and GRACE data. Leading modes of variability and long-term changes in the PDSI and percentage of dry and wet areas are discussed in section 5. A summary is given in section 6.

## 2. Data Sets

[12] Any drought index is useful only to the extent that the forcing data used to compute it can be trusted. This point is becoming increasingly relevant as demands increase for drought and other climate data with a long record length and high spatial resolution. However, historical observations are sparse or simply unavailable for temperature, precipitation, and other meteorological variables over many land areas, especially in the Southern Hemisphere and before around 1950. Some analysis data sets, such as the widely used 0.5° product (CRU TS2.1 and other versions) from the Climatic Research Unit (CRU; <http://www.cru.uea.ac.uk/cru/data>), used station data several hundred kilometers (for precipitation) to over 1000 km (for temperature) away from the grid box to derive the gridded values, or simply filled with long-term climatological values when such “nearby” observations were unavailable. The face values from this gridded data set were often used as real observations with the nominal temporal and spatial resolution to derive drought indices or drive land surface models that could lead to misleading results. Here I devoted considerable efforts to compare and derive the forcing data for calculating the PDSI and sc\_PDSI.

[13] Table 1 summarizes the data sets used in this study for calculating and evaluating the PDSI and sc\_PDSI. Although some areas (such as parts of Europe and the United States) have data for computing the PDSI and sc\_PDSI since 1850, most of the world does not have climate data before 1900, and many areas do not have data before around 1950. For computing monthly values for the (original) PDSI and sc\_PDSI using PE\_th, referred to as PDSI\_th and sc\_PDSI\_th hereafter, only monthly data for surface air temperature (T) and P are needed. Here I derived the monthly T from 1850 to 2008, as done by *Dai et al. [2004]*, by combining the CRUTEM3 anomalies [*Brohan et al., 2006*] and the CRU 1961–1990 climatology, both from <http://www.cru.uea.ac.uk/cru/data/temperature/>.

[14] For monthly P over land from 1850 to 2008, there is no single data set that covers the entire period. After evaluating various P data sets, I derived the P data by merging the monthly anomaly data from *Dai et al. [1997]* for the period 1850–1947, from *Chen et al. [2002]* for 1948–1978, and from *Huffman et al. [2009]* (Global Precipitation Climatology Project (GPCP) v2.1) for 1979–2008. The merging was done by removing the mean difference over a common data period (1979–1996) between the Huffman et al. and Chen et al. data sets from the Chen et al. P over the 1948–1978 period, and by adding the 1979–1996 mean of Huffman et al. to the P anomalies of *Dai et al.* (adjusted to be relative to the 1979–1996 mean) for 1850–1947. I noticed a large decline in the rain gauge number since 1997 in the Chen et al. data set, which led me to use the whole GPCP data set from 1979 to 2008. This is different from *Dai et al. [2004]*, who used the P data from *Chen et al. [2002]* for all years since 1948. I also examined the newly released Global Precipitation Climatology Centre (GPCC) v4 gridded land precipitation data from 1901 to 2007 ([ftp://ftp-anon.dwd.de/pub/data/gpcc/html/fulldata\\_download.html](ftp://ftp-anon.dwd.de/pub/data/gpcc/html/fulldata_download.html)). I found that for the period since around 1950, the GPCC v4 showed changes similar to our merged precipitation data, but for 1901–1949, the GPCC v4 showed different change patterns that are inconsistent with previous analyses [e.g., *Dai et al., 1997*]. Unlike *Dai et al.*

[1997], the GPCC v4 product has data over areas without rain gauges nearby, often filled with climatological values that make it difficult to assess which regions had no observations and thus should be skipped in the analysis.

[15] All the P data sets were on the same  $2.5^\circ$  latitude  $\times$   $2.5^\circ$  longitude grid as used for the PDSI calculations. The CRUTEM3 T anomaly values were on a  $5^\circ$  grid. I simply assigned the  $5^\circ$  grid-box value to the four  $2.5^\circ$  grid boxes within each  $5^\circ$  box. The CRU monthly T climatology was on a  $0.5^\circ$  grid. I simply averaged them onto the  $2.5^\circ$  grid. I realize that data for both T and P before around 1950 contain large errors or are unavailable over many regions besides Europe and the United States. I assigned a missing data code to the PDSI whenever T or P data were unavailable (mainly for years before 1948).

[16] For computing the PDSI and sc\_PDSI using the Penman-Monteith PE (PE\_pm, based on equation (4.1.14) of *Shuttleworth* [1993]), referred to as PDSI\_pm and sc\_PDSI\_pm hereafter, additional data for surface net radiation, humidity, wind speed, and air pressure are needed. There are no station-data-based analysis products for these variables, except for surface humidity for which CRU has created a  $0.5^\circ$  product from 1901 to 2002 for surface vapor pressure [*Mitchell and Jones*, 2005]. However, many land areas in the CRU product had no observations and were filled with long-term mean values. Furthermore, the station data used for the  $0.5^\circ$  CRU product were not as vigorously checked for temporal inhomogeneity as for the CRUTEM3 data set. For these reasons, I simply used the gridded data from 1948 to 2008 for surface-specific humidity, wind speed, and air pressure from the National Centers for Environmental Prediction/National Center for Atmospheric Research (NCEP/NCAR) reanalysis [*Kalnay et al.*, 1996]. In addition, we used surface net solar radiation from the Community Land Model version 3 (CLM3) simulation [*Qian et al.*, 2006], in which observed cloud cover [from *Qian et al.*, 2006] was used to estimate surface downward solar radiation. Surface net longwave radiation was estimated using surface air temperature, vapor pressure, and observed cloud fraction [*Dai et al.*, 2006] based on equation (4.2.14) of *Shuttleworth* [1993]. Since data before 1948 for these additional surface variables are not readily available over most land areas, I simply used the long-term mean values for years before 1948. Thus, the PDSI\_pm and sc\_PDSI\_pm before 1948 contain no additional variations compared to PDSI\_th and sc\_PDSI\_th, respectively. I realize that large uncertainties likely exist in these surface data, especially for surface wind speed and radiation, as high-quality data for these fields are unavailable over the global land. Because of this, the PDSI\_pm and sc\_PDSI\_pm results may not fully reflect the impact of the actual changes in wind speed [*Roderick et al.*, 2007] and radiation on aridity [*Donohue et al.*, 2010] since 1950.

[17] As in the studies by *Dai et al.* [1998, 2004], I used the soil texture-based estimate of the water-holding capacity map from *Webb et al.* [1993]. Tests showed [*Dai et al.*, 1998] that the PDSI is not sensitive to the holding capacity values, presumably due to the normalization used in the Palmer model.

[18] Drought is often associated with dry soils and below-normal streamflow [*Dai*, 2011]. Thus, I evaluate the performance of the PDSI and sc\_PDSI as a measure of drought by correlating area-averaged PDSI and sc\_PDSI values with

available records of soil moisture observed over Illinois in the United States and regions in Eurasia [*Robock et al.*, 2000] and observed streamflow for the world's largest 230 rivers [*Dai et al.*, 2009] (Table 1). Here I also did a correlative analysis between the monthly anomalies of GRACE satellite-observed liquid water equivalent thickness [*Swenson and Wahr*, 2006] and the various forms of the PDSI. Although the GRACE satellite measures variations in both groundwater and soil moisture [*Swenson et al.*, 2006], we expect a positive correlation between the two as severe droughts can reduce both soil moisture and groundwater levels.

### 3. Characteristics of Different Forms of the PDSI

#### 3.1. Formulation of the PDSI

[19] Here I briefly describe the relevant aspects of the PDSI and sc\_PDSI formulations. More details can be found in the studies by *Palmer* [1965], *Alley* [1984], *Karl* [1986], and *Wells et al.* [2004].

[20] Besides P, *Palmer* [1965] considered four other surface water fluxes: E, recharge to soils (R), runoff (RO), and water loss to the soil layers (L), and their potential values PE, PR, PRO, and PL, respectively. Then Palmer introduced the concept of the climatically appropriate for existing conditions (CAFEC) values. To do that, he first defined the following water-balance coefficients calculated using local climate (often over a calibration period, which is 1950–1979 in this study) for each month *i*:

$$\alpha_i = \frac{\overline{E}_i}{\overline{PE}_i} \quad \beta_i = \frac{\overline{R}_i}{\overline{PR}_i} \quad \gamma_i = \frac{\overline{RO}_i}{\overline{PRO}_i} \quad \delta_i = \frac{\overline{L}_i}{\overline{PL}_i}, \quad (1)$$

where the overbar indicates averaging over the calibration period. Thus, these coefficients represent the ratio of the long-term mean values between a water flux and its potential value. The CAFEC values are simply the product of the potential value of a water flux times its coefficient, e.g.,  $\alpha_i$  PE for CAFEC evapotranspiration. In particular, the CAFEC precipitation ( $\hat{P}$ ), which represents the amount of precipitation needed to maintain a normal soil moisture level for a given time, is defined as

$$\hat{P} = \alpha_i PE + \beta_i PR + \gamma_i PRO - \delta_i PL. \quad (2)$$

The difference between the actual precipitation in a given month and the computed  $\hat{P}$  for the same month is the moisture departure ( $D = P - \hat{P}$ ) for the month. Obviously, a given value of  $D$  can have different meanings for the surface water balance at different locations and different times of the year. To correct that, Palmer multiplied  $D$  by a climatic characteristic coefficient  $K$  to derive the moisture anomaly index or the Z index ( $Z = DK$ ), where  $K$  for month *i* is defined by Palmer using data from the central United States as follows:

$$K_i = K_o \quad K'_i = \frac{17.67}{\sum_{i=1}^{12} \overline{D}_i} K'_i \quad \text{and} \\ K'_i = 1.5 \log_{10} \left( \frac{\frac{\overline{PE}_i + \overline{R}_i + \overline{RO}_i}{\overline{P}_i + \overline{L}_i} + 2.8}{\overline{D}_i} \right) + 0.5. \quad (3)$$

The Z index is then used to compute the PDSI value for time  $t$  ( $X_t$ ):

$$X_t = p X_{t-1} + q Z_t = 0.897 X_{t-1} + Z_t/3, \quad (4)$$

where  $X_{t-1}$  is the PDSI for the previous month. The use of  $K_i$  is to allow comparisons of PDSI values over different time and space. The  $p$  and  $q$  coefficients in (4) are called duration factors, which determine how sensitive the PDSI is to the monthly moisture anomaly  $Z_t$  and how much autocorrelation the PDSI has. Palmer [1965] derived the values of  $p = 0.897$  and  $q = 1/3$  using the linear slope between the length and severity of the most extreme droughts that he studied in Kansas and Iowa.

[21] To make the PDSI more comparable spatially, Wells *et al.* [2004] proposed a new method to calculate  $K$  (more specifically,  $K_o$  in (3)),  $p$ , and  $q$  using local climate conditions, so that the PDSI has more comparable histograms across different locations and the duration factors  $p$  and  $q$  reflect the local slope between the length and severity of the most extreme droughts. However, one still needs to make certain choices regarding the exact length over which the regression for the slope is done and how the extreme drought spells are selected. Wells *et al.* [2004] did not discuss these issues. I tested three different methods for doing the length versus severity regression that determines the  $p$  and  $q$  values and found that the results are not very sensitive to these methods (see Appendix A for details). Here I used the results from one of the methods (i.e., method 2) in the following.

### 3.2. Potential Evapotranspiration

[22] Another key aspect of the PDSI is how the PE is computed in the Palmer model. Mainly based on practical considerations, Palmer [1965] used the Thornthwaite [1948] equation to compute the PE as a function of monthly mean surface air temperature, latitude, and month. There are criticisms of the PDSI computed using the PE\_th because the PE\_th may overestimate the impact of surface temperature on PE [Trenberth *et al.*, 2007, p. 261; Hobbins *et al.*, 2008]. To investigate the impact of different PE calculations on the PDSI and sc\_PDSI, here I also used the more physically based Penman-Monteith equation to compute the PE. The formulations for the PE\_th and PE\_pm are given in Appendix B.

[23] Figures 1a and 1b show that the PE\_th and PE\_pm exhibit different decadal change patterns from 1950–1969 to 1985–2004, and the impact without temperature changes (Figures 1c and 1d) also differs substantially for the two different PE estimates. However, for the actual evapotranspiration (Figures 1e–1h) estimated by the Palmer model, the choice of the PE formulation has relatively small effects, mainly because E is often limited by the available moisture on the ground. Because it is E, not PE, that affects the surface water balance, and also because of the normalization used in the Palmer model (see equations (1)–(3)), the PDSI of the 20th century is not very sensitive to the choice of the PE parameterization, as shown below and by van der Schrier *et al.* [2011]. However, for the model-projected 21st century climate with large increases in surface temperature, I found that the PE\_th overestimates the impact of rising temperatures and results in much larger PDSI decreases than using PE\_pm [Dai, 2011]. These findings are consistent

with conclusions of Burke *et al.* [2006] and van der Schrier *et al.* [2011], who also found that the PDSI of the 20th century was similar when either PE\_th or PE\_pm was used.

### 3.3. Histograms of the PDSI

[24] Figures 2 and 3 compare the histograms of the monthly PDSI\_pm and sc\_PDSI\_pm, respectively, at nine grid boxes around the world during 1900–1979. Some boxes may not have data for the earlier decades of the period, and years after 1979 are not included because of the recent drying trend. Histograms for PDSI\_th (sc\_PDSI\_th) are not very different from those for PDSI\_pm (sc\_PDSI\_pm) at most of the locations. It can be seen that the PDSI and sc\_PDSI ranges vary from location to location, and the shape of the distributions can differ substantially from Gaussian at some locations such as the Amazonian and southern Indian boxes. The normalization to local climate in sc\_PDSI improves the symmetry of the distributions, but it is still not Gaussian at some locations (e.g., the Amazon), and this problem exists even for the histograms of the calibration period (1950–1979). The value range of the sc\_PDSI becomes more comparable among the different locations, generally within -6 to +6, whereas the range for the original PDSI varies considerably from one location to another, making it less comparable spatially. Thus, the sc\_PDSI is indeed improved over the original PDSI in terms of spatial comparability, but it is still not symmetrically distributed around the neutral (i.e., zero) line at some locations.

## 4. Evaluation of the PDSI

[25] As a drought index, the PDSI and sc\_PDSI, when averaged over a region, should correlate with other observed measures of drought, such as soil moisture and streamflow, which are often used to define agricultural and hydrological droughts, respectively [Dai, 2011]. Figures 4 and 5 summarize the correlation between the available data of soil moisture monthly anomalies (Table 1) and the different forms of the PDSI averaged over various regions in Eurasia and the United States. It can be seen that all the forms of the PDSI are significantly correlated with the observed soil moisture variations within the top 1 m depth, especially over Illinois ( $r$  up to 0.84), parts of the former Soviet Union ( $r$  up to 0.77), and East China ( $r$  up to 0.73). Furthermore, the correlations for the four different forms of the PDSI are similar, perhaps except for PDSI\_pm over Illinois, which has a lower correlation than the other three forms.

[26] Figures 6–8 summarize the correlation between observed yearly streamflow and the different forms of the PDSI averaged over each of the world's 230 largest river basins that I can define and for which I have streamflow data [see Dai *et al.*, 2009]. It is necessary to use yearly data as precipitation may take weeks to months to contribute to the streamflow. It can be seen (Figure 6) that the basin-averaged PDSI\_th and sc\_PDSI\_pm both covary with the observed streamflow variations on interannual to decadal time scales for the world's largest rivers, except for Yenisey where the streamflow trend is not reflected in precipitation [Dai *et al.*, 2009] and thus also not reflected by the PDSI. Figure 7 shows that basin-averaged PDSI\_pm (and the other forms) is significantly correlated ( $r = 0.4$ –0.9) with the observed streamflow over the majority (87%) of the top 230 rivers in the world. The low correlation over the remaining 13% of the river basins

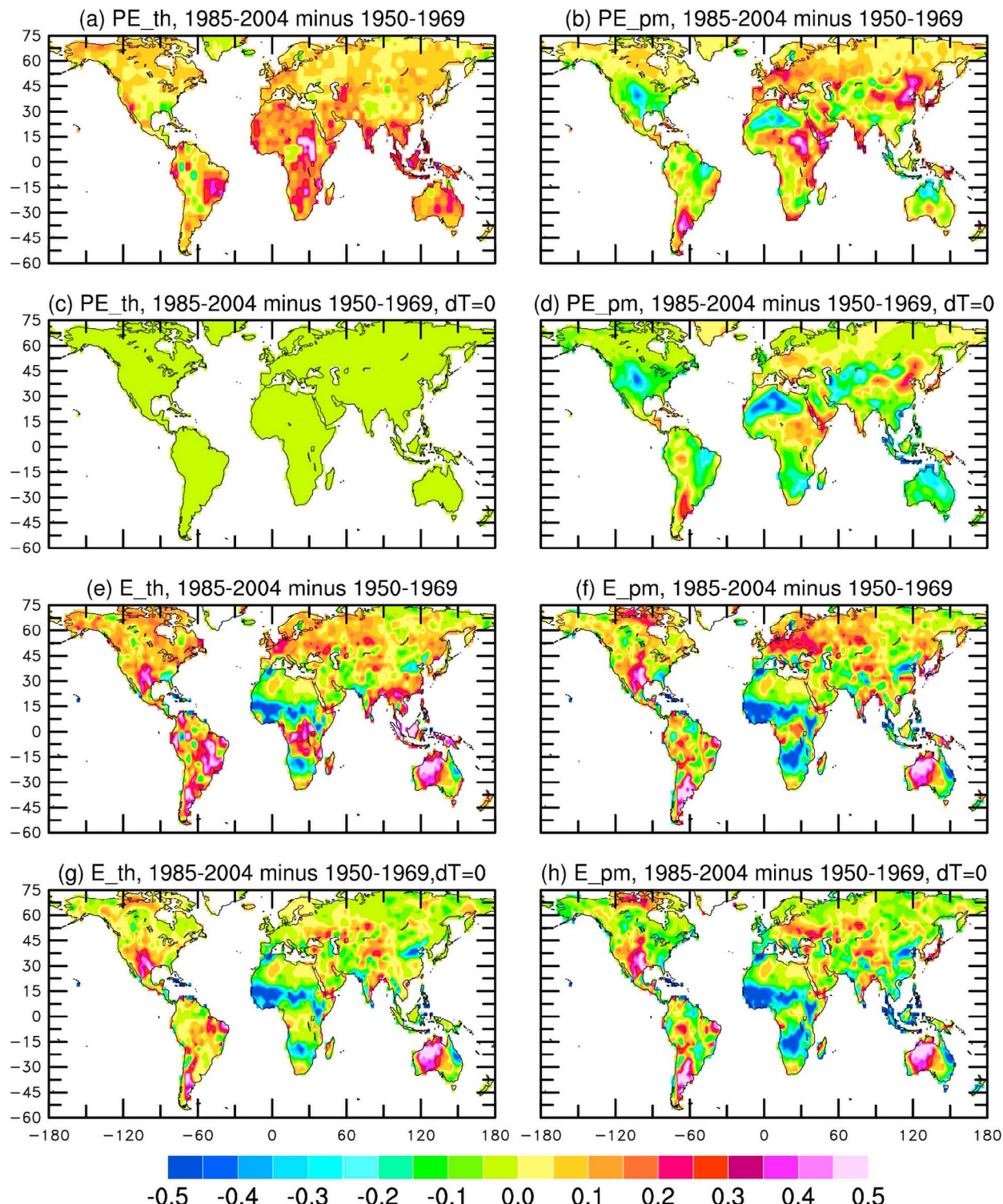


**Figure 1.** Changes in (a-d) potential evapotranspiration (mm/d) and (e-h) evapotranspiration (in units of 0.5 mm/d) from 1950–1969 to 1985–2004 calculated using the Thornthwaite (Figures 1a, 1c, 1e, and 1g) and Penman-Monteith (Figures 1b, 1d, 1f, and 1h) equations. Figures 1a, 1b, 1e, and 1f are cases with all atmospheric forcings, while Figures 1c, 1d, 1g, and 1h are cases with all except the temperature changes.

## Histograms of Monthly PDSI: 1900–1979

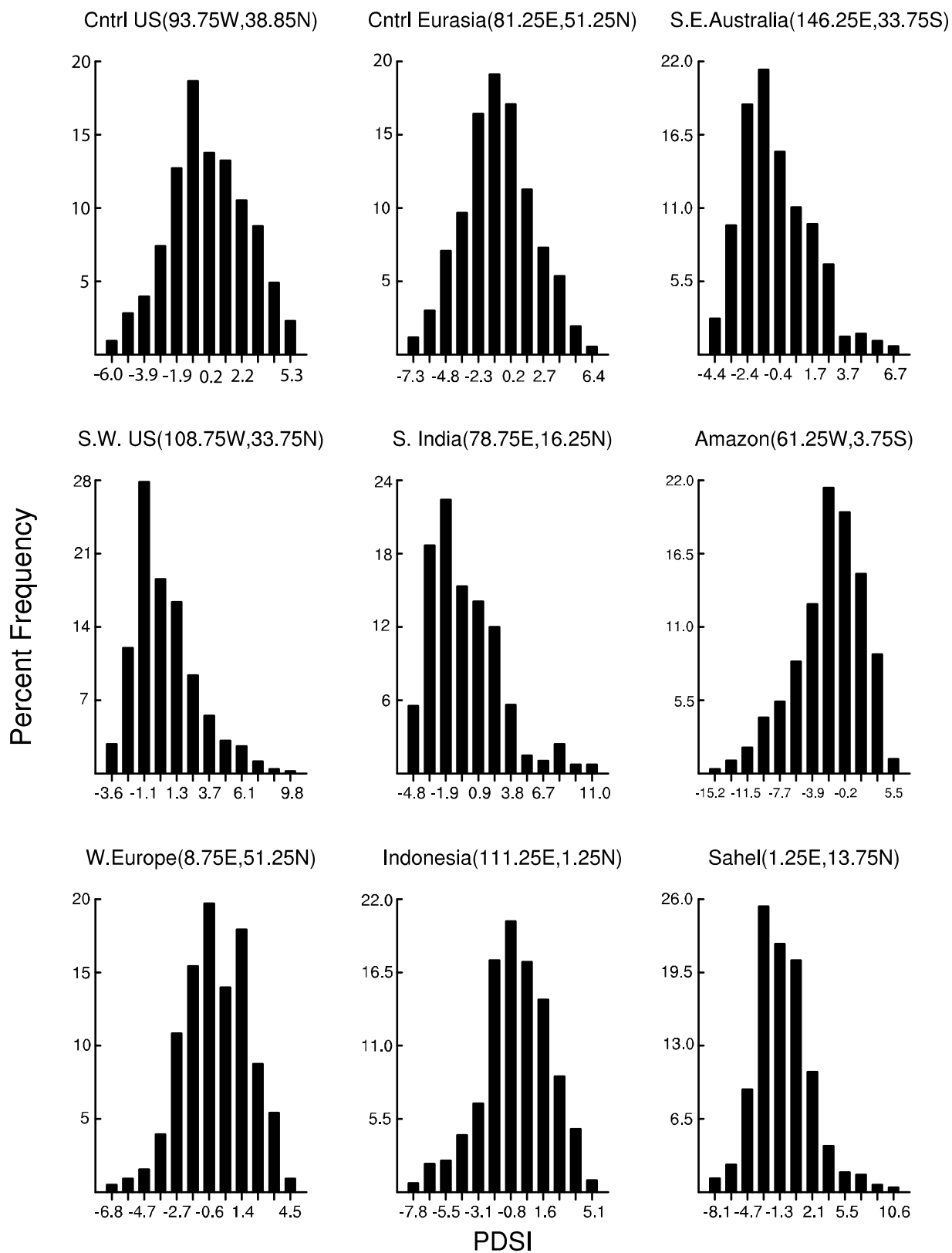


**Figure 2.** Histograms of monthly PDSI<sub>pm</sub> during 1900–1979 at nine individual  $2.5^\circ \times 2.5^\circ$  grid boxes. The calibration period is 1950–1979.

## Histograms of Monthly SC-PDSI: 1900–1979

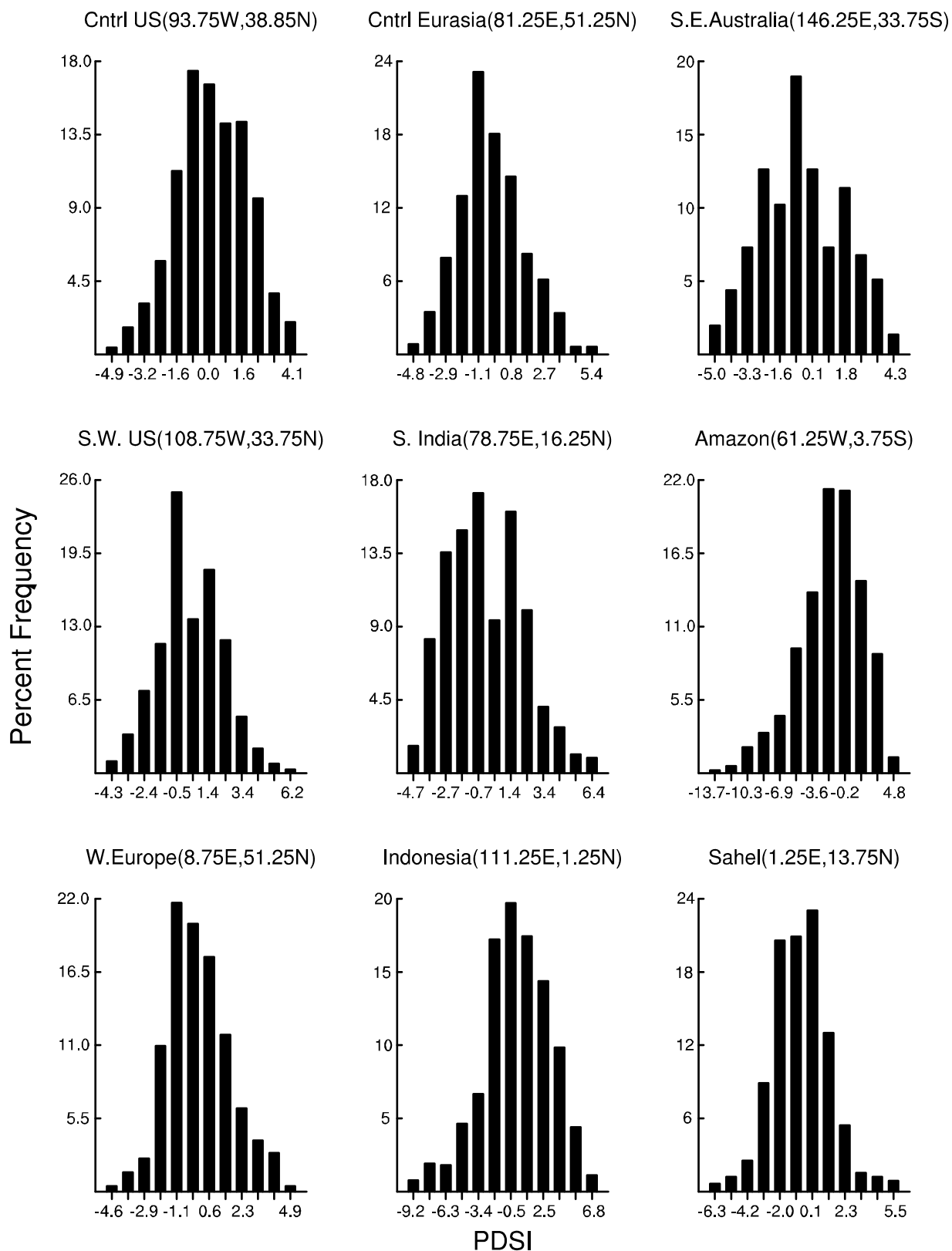


**Figure 3.** Same as Figure 2 but for sc\_PDSI\_pm. To increase the comparability of the shapes of the histograms in Figures 2 and 3, the same number of bins (not the same intervals for the bins) is used in Figures 2 and 3 given the same sample size and different value ranges between the PDSI\_pm and sc\_PDSI\_pm cases.

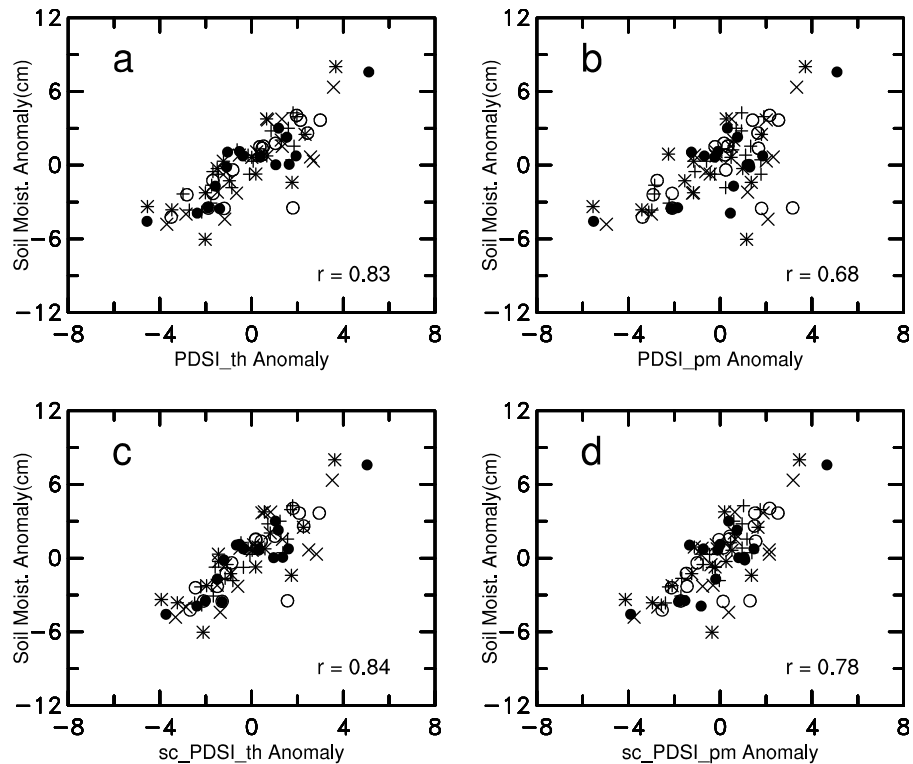


**Figure 4.** Scatterplots of monthly anomalies over Illinois from 1981 to 2001 of observed soil moisture content within the top 0.9 m depth against the PDSI with PE calculated using the (a) Thornthwaite (PDSI\_th) and (b) Penman-Monteith (PDSI\_pm) equations, (c) self-calibrated PDSI with Thornthwaite PE (sc\_PDSI\_th), and (d) self-calibrated PDSI with Penman-Monteith PE (sc\_PDSI\_pm). The correlation coefficient ( $r$ ) is also shown. The plus, open circle, cross, asterisk, and solid circle are for months 5, 6, 7, 8, and 9, respectively. There are insufficient soil moisture data for the other months.

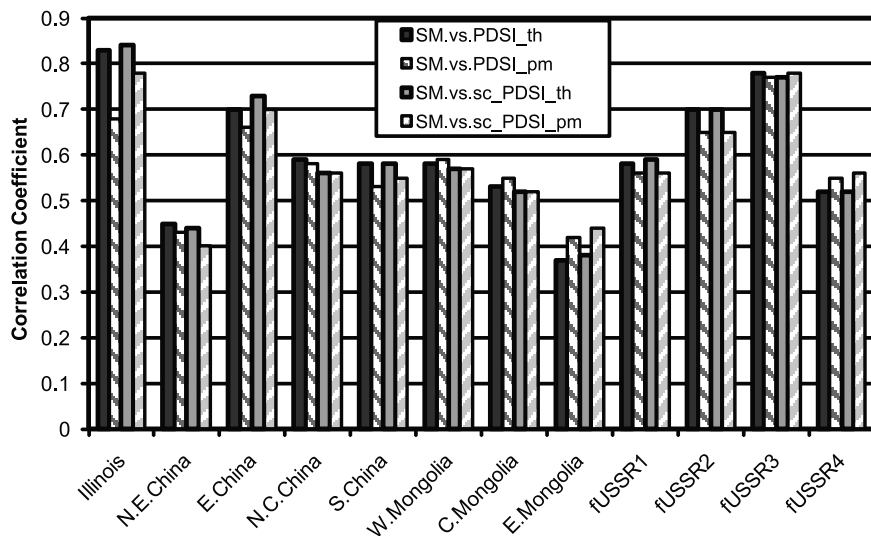


**Figure 5.** Correlation coefficients between monthly anomalies of observed soil moisture (see Table 1) and four different forms of the PDSI (see Figure 6 for their definitions) averaged over 12 regions where soil moisture data are available. Some cold months have no soil moisture data and are thus not included in the calculations. See Table 2 of *Dai et al.* [2004] for the definition of the regions, the number of stations with soil moisture observations, and the months included.

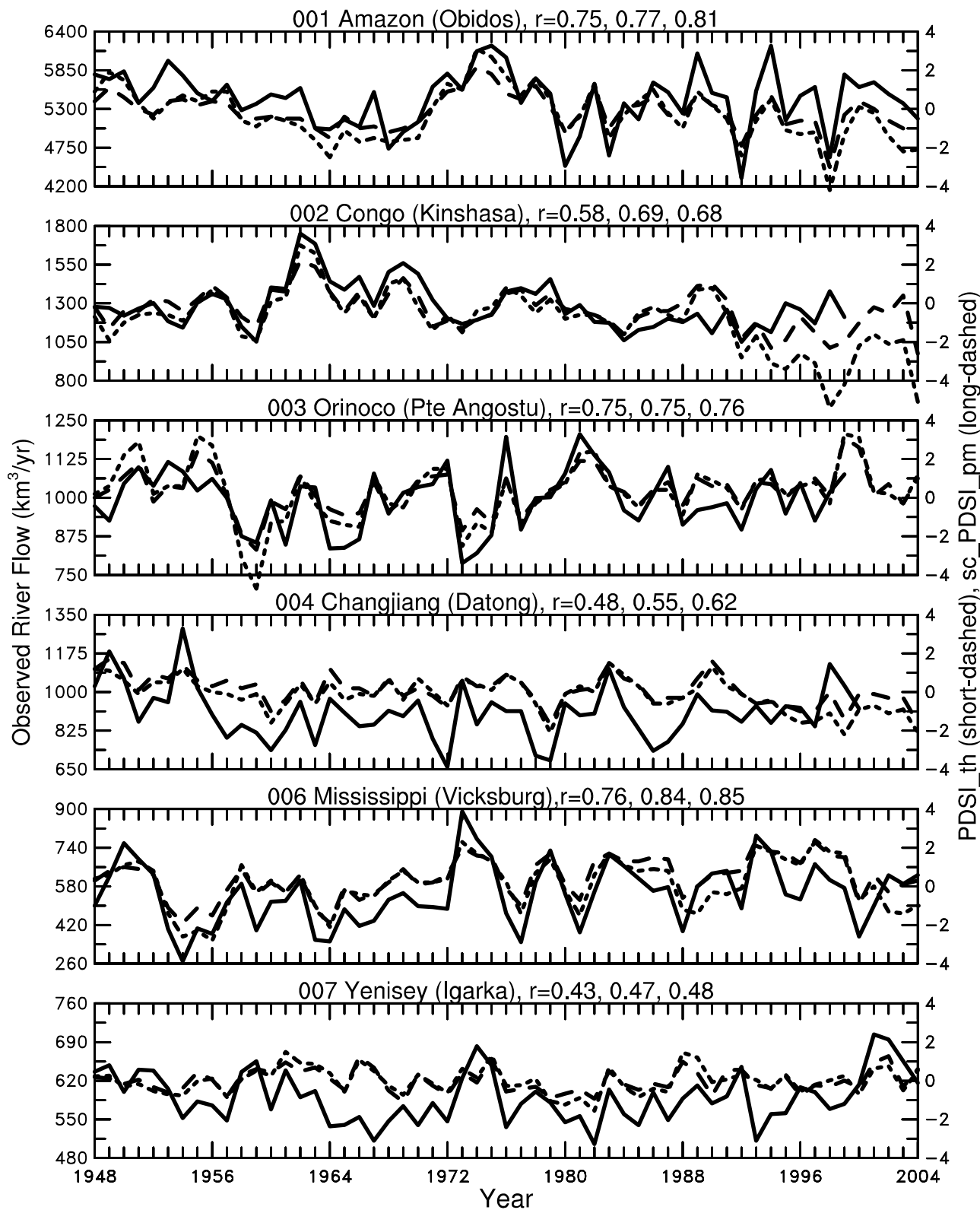


**Figure 6.** Time series of observed water-year (1 October to 30 September) streamflow ( $\text{km}^3 \text{ yr}^{-1}$ , solid line) at the farthest downstream station for the world's six largest rivers compared with basin-averaged PDSI<sub>th</sub> (short dashed line) and sc\_PDSI<sub>pm</sub> (long dashed line). The lines for PDSI<sub>pm</sub> are similar to those for sc\_PDSI<sub>pm</sub> and thus are not shown. The correlation coefficients ( $r$ ) are for streamflow versus, from left to right, PDSI<sub>th</sub>, PDSI<sub>pm</sub>, and sc\_PDSI<sub>pm</sub>. Note the streamflow for Yenisey was detrended before the correlation analysis (same for Figures 7 and 8).

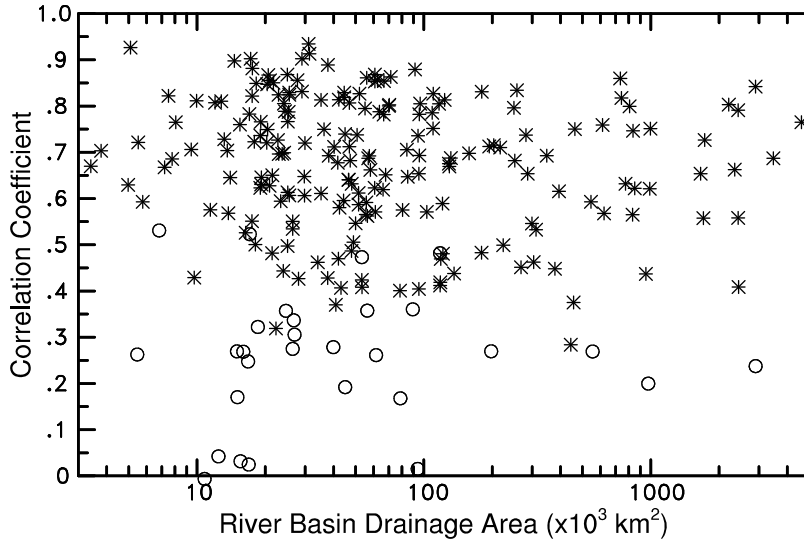


**Figure 7.** Scatterplot of the correlation coefficient between observed downstream water-year river flow and PDSI<sub>pm</sub> during 1948–2004 against the river drainage area for the world's top 230 rivers. Asterisks (~200) indicate the correlation is statistically significant at the 5% level, while the open circles (~30) are insignificant. Plots for PDSI<sub>th</sub>, sc\_PDSI<sub>th</sub>, and sc\_PDSI<sub>pm</sub> are similar.

could result from factors not considered in the Palmer model, such as human withdrawal of stream water or changes in land water storage. Figure 8 shows that the low correlation exists mainly in the arid areas, where direct human influence on streamflow is large [Milliman *et al.*, 2008], and Siberia, where permafrost thawing may have contributed to observed streamflow changes [Dai *et al.*, 2009]. Figure 8 further illustrates that the different forms of the PDSI correlate similarly with observed streamflow for world's largest river basins. Furthermore, the PDSI is correlated with observed streamflow over many high-latitude regions, despite that snow and other cold land processes are not explicitly treated in the Palmer model. This result is consistent with the significant correlation with observed soil moisture over Russia, Mongolia, and northern China (Figure 5).

[27] Figure 9 shows the maps of the correlation coefficient ( $r$ ) from April 2002 to December 2008 between the monthly anomalies of GRACE satellite-observed liquid water equivalent thickness and the PDSI<sub>th</sub>, PDSI<sub>pm</sub>, and sc\_PDSI<sub>pm</sub> (similar for sc\_PDSI<sub>th</sub>; not shown). It can be seen that the different forms of the PDSI are similarly and positively correlated with the variations in GRACE-measured water thickness over most land areas, with the  $r$  ranging from 0.4 to 0.8. The correlation is low (below 0.4) and insignificant over northern Africa, northern India, parts of the Middle East, central and northern Asia, and a few other areas. Since this is a correlation at the local grid box level, we expect some areas to have lower correlations because of poor sampling of precipitation and other forcing data used for computing the PDSI. Also, continuing human withdrawal of groundwater for domestic, agricultural, and other usages in arid regions such as central North China, northern India, and the Middle East likely have affected the GRACE measurements, while it has little effect on the climate-derived PDSI values. Tests showed that the correlation becomes positive over northern

India when the GRACE data were detrended. This suggests that the GRACE data contain human-induced variations and changes that are not considered in the climate-driven PDSI values. Thus, low correlations should be expected over arid and other regions where such human influences are significant.

[28] Thus, I conclude that the different forms of the PDSI can all capture many of the observed variations and changes in soil moisture and streamflow during the latter half of the 20th century around the world including many cold regions, and neither the use of Penman-Monteith PE nor the self-calibration proposed by Wells *et al.* [2004] significantly improves the PDSI's ability to capture the observed soil moisture and streamflow variations. Furthermore, the different forms of the PDSIs are similarly correlated with satellite-observed variations in terrestrial water storage during recent years. As stated above, however, the sc\_PDSI does become more comparable spatially, and the use of PE<sub>pm</sub> is necessary for the model-projected 21st climate.

## 5. Historical Variations and Changes in the PDSI

### 5.1. Leading Modes of Variability

[29] Figure 10 shows the two leading modes of variability from an empirical orthogonal function (EOF) analysis of monthly sc\_PDSI<sub>pm</sub> (similar for PDSI<sub>pm</sub>) from 1900 to 2008. These modes are comparable to those for the original PDSI (i.e., PDSI<sub>th</sub>) shown previously by Dai *et al.* [2004] and Dai [2011], although the red colors (i.e., drying) for EOF 1 (Figure 10b) are slightly less widespread compared with the PDSI<sub>th</sub> case. In other words, the use of the PE<sub>pm</sub> slightly reduces the drying effect of recent warming over land. Nevertheless, the first mode still represents a long-term trend (Figure 10a; mainly since ~1950) of drying over Africa, East and South Asia, southwestern Europe, and eastern Australia

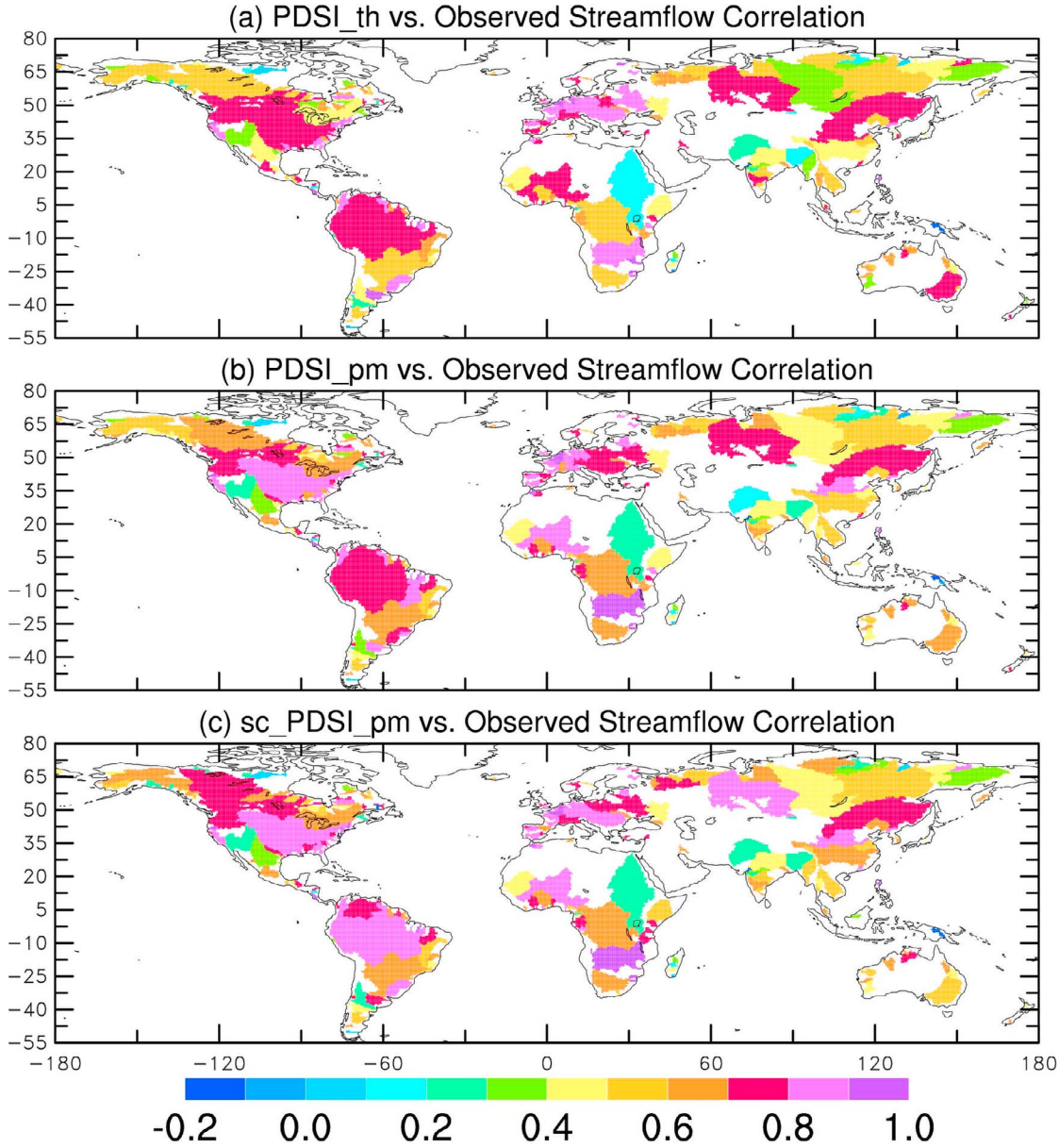


**Figure 8.** Maps of correlation coefficients between the observed water-year downstream river flow and (a) PDSI<sub>th</sub>, (b) PDSI<sub>pm</sub>, and (c) sc\_PDSI<sub>pm</sub> averaged over the world's large river basins during 1948–2004. Blank areas indicate a lack of sufficient data.

and wetting over the continental United States, Argentina, northern Europe, and parts of northern Asia. The second mode is associated with the El Niño–Southern Oscillation (ENSO), since its temporal time series is correlated with an ENSO index (Figure 10c, red line) and its spatial patterns (Figure 10d) is comparable to those of ENSO-induced precipitation [Dai and Wigley, 2000]. This ENSO-induced mode is very stable in all the forms of the PDSI, as well as in the previous versions of the PDSI [Dai *et al.*, 2004; Dai, 2011], although the principal component (PC) series since the late 1990s is slightly lower than expected from the ENSO index (Figure 10c). Thus, the two leading EOFs represent two distinct modes of variability in the global PDSI that are inde-

pendent of the choice of the forcing data sets and the form of the PDSI.

### 5.2. Long-Term Trend in Global Aridity and the Effect of Surface Warming

[30] In this subsection, I focus on the period after 1950 since many of the global land areas have no climate records before about 1950, except western Europe, the United States, and a few other regions (see section 5.3). Figures 11a–11d show that the trend patterns during 1950–2008 in the four forms of the PDSI are similar, although the magnitude of the drying trend over many regions (e.g., Africa and East Asia) is smaller for the self-calibrated PDSI than for the original

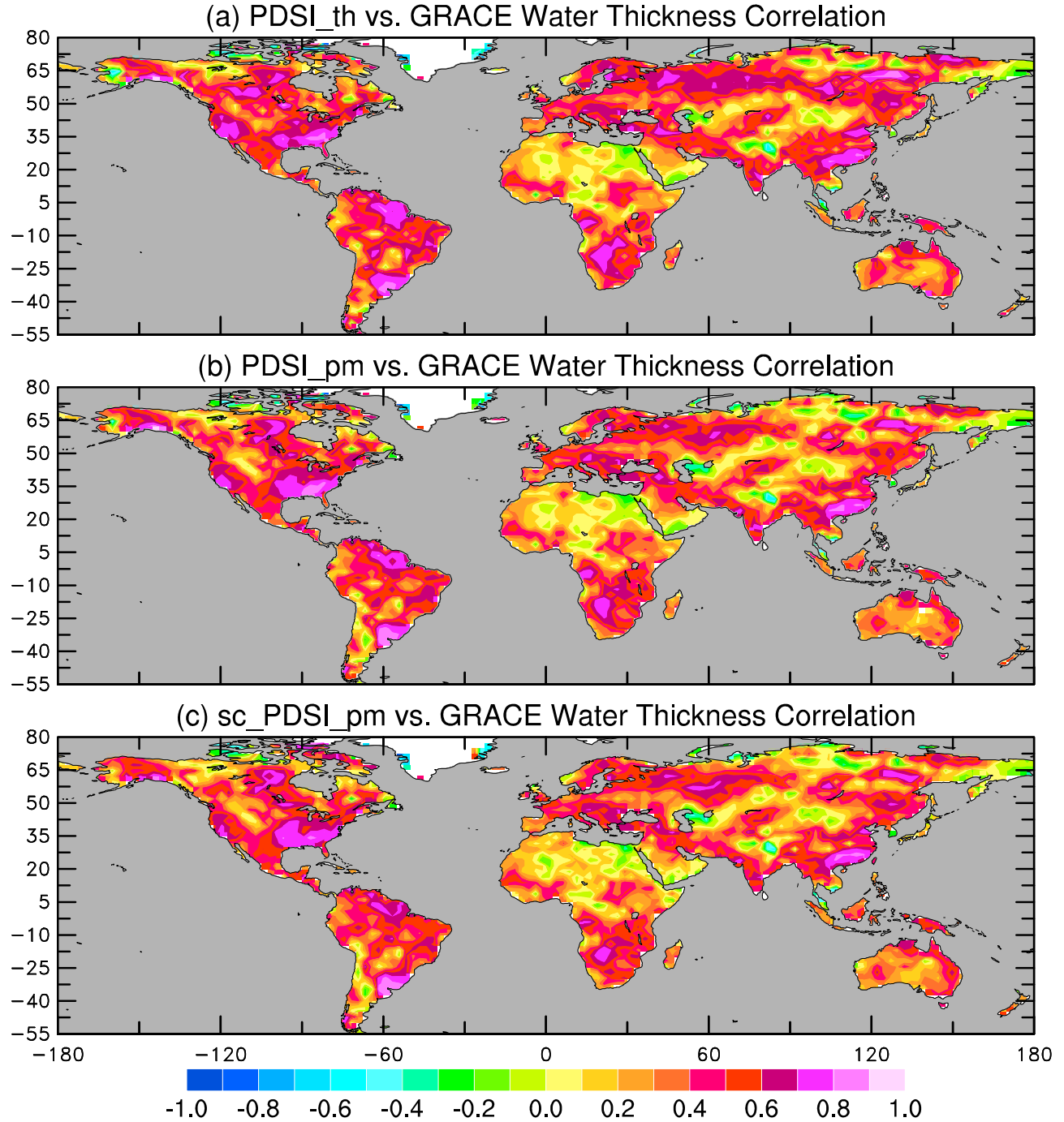


**Figure 9.** Maps of correlation coefficients between monthly anomalies of GRACE satellite-observed liquid water equivalent thickness and (a) PDSI\_th, (b) PDSI\_pm, and (c) sc\_PDSI\_pm at each  $2.5^\circ \times 2.5^\circ$  land box from April 2002 to December 2008. Values above about 0.4 or below -0.4 are statistically significant at the 5% level.

PDSI. This results mainly from the reduced PDSI range during the self-calibration (see Figures 2 and 3). Furthermore, the use of the two different PE formulations results in only small differences in the PDSI trends, with slightly less drying (e.g., over central South America) for the PE\_pm cases. This result is consistent with that of *van der Schrier et al. [2011]*, who showed very small differences in the trends of their

sc\_PDSI\_th and sc\_PDSI\_pm during 1901–2006. Also, many of the trend patterns (e.g., drying over West Africa, southwestern Europe, and East Asia and wetting over Argentina and most of western Australia) are consistent between our Figures 11c and 11d and their Figure 3, although more quantitative comparisons require examining for the same time period.

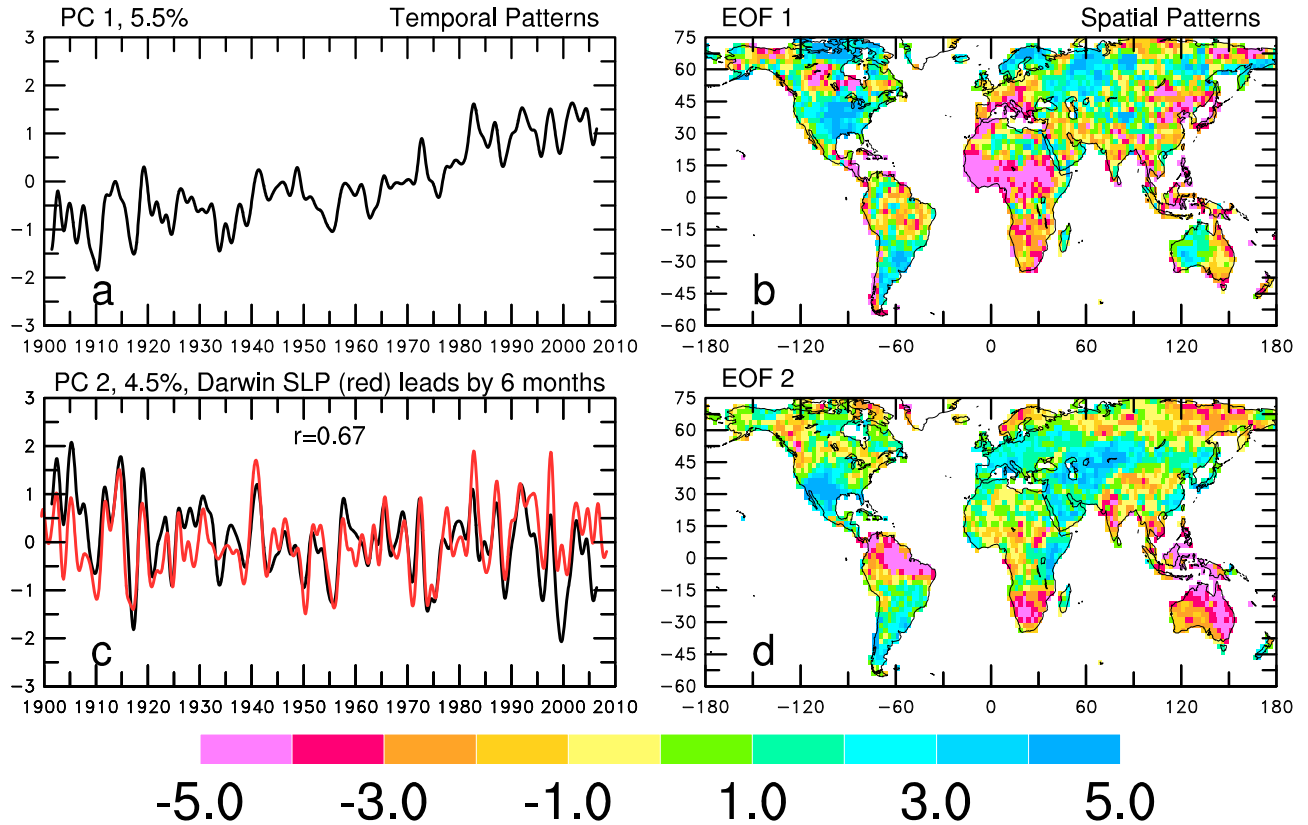


**Figure 10.** (a, c) Temporal (black) and (b, d) spatial patterns of the two leading EOFs of monthly sc\_PDSI\_pm from 1900 to 2008 (normalized by its standard deviation prior to the EOF analysis). Red (blue) areas are dry (wet) for a positive temporal coefficient on the corresponding PC time series (e.g., the red (blue) areas in Figure 10b represent a drying (moistening) trend whose temporal pattern is shown in Figure 10a). Variations on <2 year time scales were filtered out in plotting Figures 10a and 10c (but retained in the EOF analysis). Also shown in Figure 10c is the normalized Darwin mean sea level pressure anomaly shifted to the right (i.e., lead) by 6 months to obtain a maximum correlation ( $r = 0.67$ ) with the PC 2 time series. The percentage variance explained by the EOF is shown at the top of Figures 10a and 10c. The product of the PC and EOF coefficients is the sc\_PDSI\_pm anomaly (in units of 0.1 SD) represented by the EOF mode. Similar PCs and EOFs are seen in PDSI\_pm and PDSI\_th.

[31] All four forms of the PDSI show widespread drying during 1950–2008 over much of Africa, Asia, southern Europe, eastern Australia, midlatitude Canada, and south-eastern Brazil, whereas much of the continental United States, Argentina, western Australia, and the Tibetan Plateau has become wetter from 1950 to 2008. These long-term trends may differ from what has happened during the most recent years. For example, over the United States, drought has become more widespread during the last 10 years (see below), which is a reversal of the longer-term trend. The drying trend over West and central Africa and East China reaches  $-2$  to  $-4$  per 50 years, which is large considering that drought starts when the PDSI is below  $-1$  [Palmer, 1965]. The PDSI drying patterns over Africa, southeastern Asia, eastern Australia, the Mediterranean region, and midlatitude Canada are qualitatively consistent with the observed streamflow decreases over these regions (see Figure 5c of Dai [2011]).

[32] To estimate the direct impact of recent warming on the PDSI trends, I computed the four forms of the PDSI with

all the forcing except temperature changes, i.e., monthly temperature climatology was used for this  $dT = 0$  case. I realize that in the real world, changes in precipitation and other surface fields are coupled to temperature changes. Here I used the  $dT = 0$  case only to illustrate the direct impact of recent warming on PDSI through its influence on PE.

[33] Figure 11 compares the 1950–2008 trend patterns between the all forcing and  $dT = 0$  cases. It can be seen that without the surface warming, most of the drying (i.e., red areas) seen in the all forcing case (Figures 11a–11d) disappears in the  $dT = 0$  case (Figures 11e–11h), except for some areas in Africa, East Asia, and eastern Australia, where the drying resulted, to a large extent, from precipitation decreases. Without the effect of surface warming, most of the land areas in Eurasia and North and South America would have become wetter (Figures 11e–11h). For the PDSI\_pm and sc\_PDSI\_pm cases, this wetting trend is slightly enhanced, compared with the PDSI\_th and sc\_PDSI\_th cases (in which surface humidity is not part of

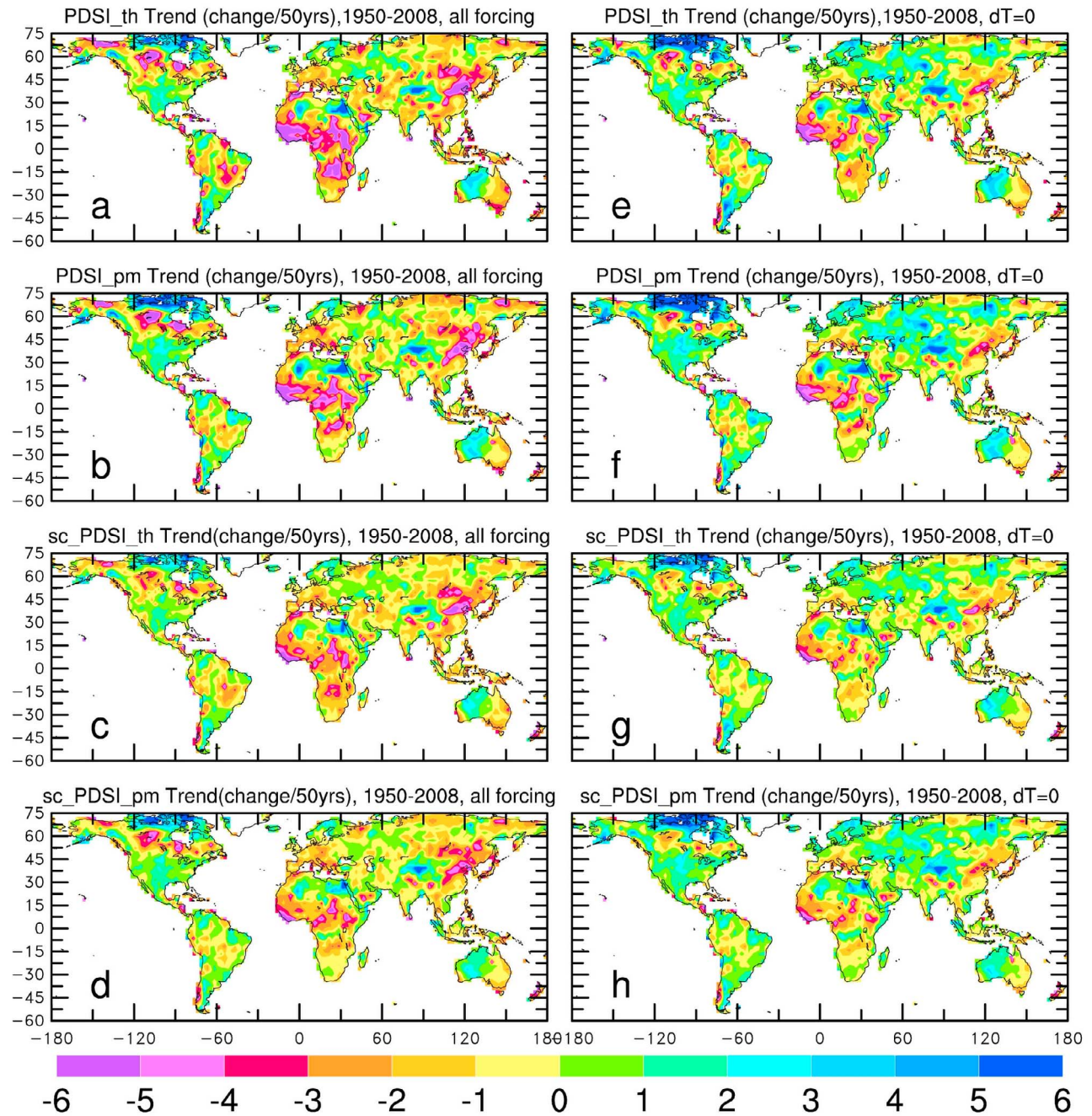


**Figure 11.** Trend maps (red, drying, change per 50 years) in the four forms of the annual PDSI from 1950 to 2008 computed using (a, b, c, d) all forcing data and (e, f, g, h) all but no temperature changes for PDSI\_th (Figures 11a and 11e), PDSI\_pm (Figures 11b and 11f), sc\_PDSI\_th (Figures 11c and 11g), and sc\_PDSI\_pm (Figures 11d and 11h).

the forcing), by the decreased evapotranspiration because of reduced water vapor deficits as surface vapor pressure increases in the forcing data while the saturation vapor pressure was fixed (to that for climatological temperature). This, of course, cannot happen in the real world as the surface-specific humidity and temperature are tightly coupled [Dai, 2006]. Nevertheless, the similar differences between the all forcing and  $dT = 0$  cases for all four PDSI forms shown in

Figure 11 suggest that recent warming, rather than precipitation and other changes, is responsible for much of the drying trend over many land areas.

[34] The effect of recent warming on the PDSI is further illustrated in Figure 12, which shows the PDSI difference between the all forcing and  $dT = 0$  cases averaged over 2000–2008. For all four forms of the PDSI, the differences are largest over central and northern Eurasia, northern North

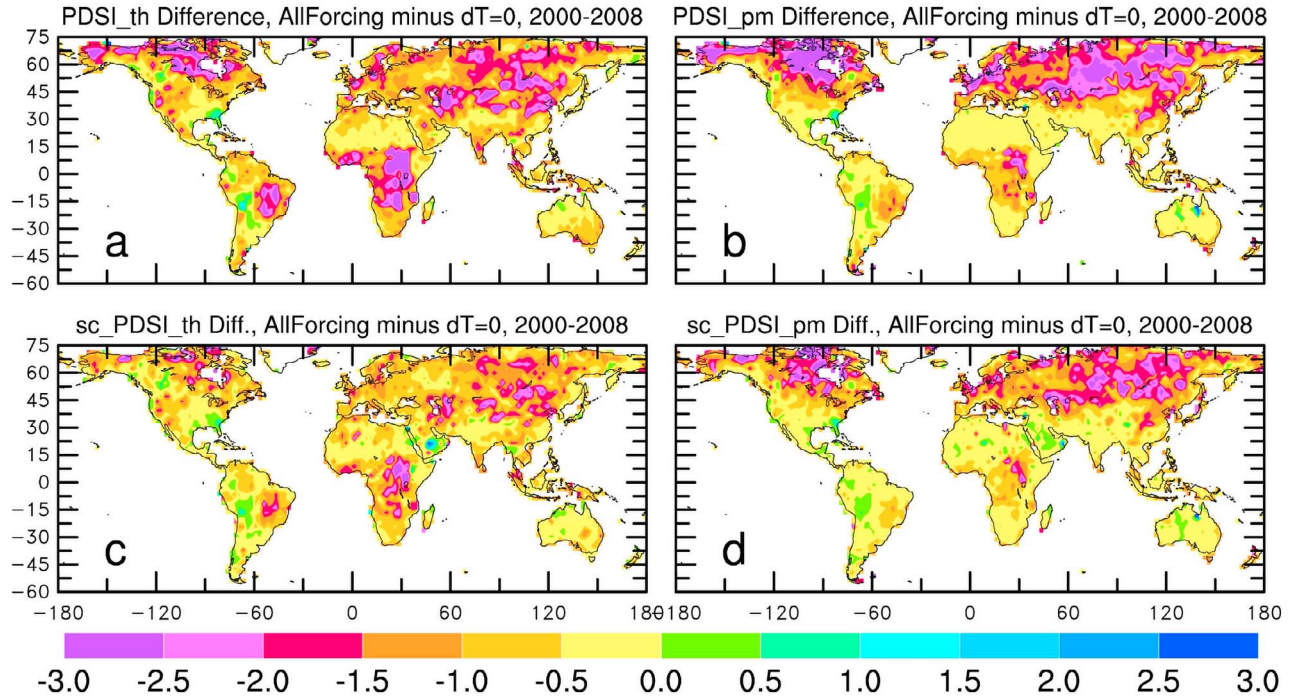


**Figure 12.** Difference of the four forms of the PDSI between the all forcing case and the  $dT = 0$  case averaged over 2000–2008: (a) PDSI\_th case, (b) PDSI\_pm case, (c) sc\_PDSI\_th case, and (d) sc\_PDSI\_pm case.

America, and parts of Africa, where surface warming has been largest (see Figure 5a of *Dai* [2011]). The differences are smaller for the self-calibrated PDSI than the original PDSI for both the PE\_th and PE\_pm cases. This is expected because the self-calibration reduces the range of the PDSI values as mentioned in section 3. Also, the PE\_pm cases (Figures 12b and 12d) show larger differences than their respective cases using PE\_th (Figures 12a and 12c). This is due to the unintended effect of water vapor deficit under the  $dT = 0$  case, which slightly increases the PDSI\_pm and sc\_PDSI\_pm for the  $dT = 0$  case, as pointed out for Figure 11.

[35] Figure 13a (colored solid lines) shows that the global land averaged annual values for the various forms of the PDSI exhibit substantial decadal variations from the 1950s to the 1970s, with negative anomalies in the 1960s and higher values in the 1950s and 1970s. Thereafter, a steady downward (i.e., drying) trend is evident in all the forms of the PDSI. The drying trend since the late 1970s is largest for the PDSI\_th, followed by the sc\_PDSI\_th (not shown in Figure 13, but it is only slightly above the red solid line from 1980 to 2008), with the PDSI\_pm and sc\_PDSI\_pm showing weaker drying trends. Figure 13a (black solid line) also shows the global land averaged annual time series of top-1 m soil moisture content simulated by a comprehensive land surface model (namely, CLM3) forced by observation-based historical forcing data [see *Qian et al.*, 2006]. The simulated soil moisture exhibits multiyear and decadal variations and a drying trend since the 1970s similar to those for the PDSI curves, although the soil moisture curve, which ends in 2004, shows an apparent recovery since the late 1990s. This may result from the use of slightly different precipitation forcing

for the land model [see *Qian et al.*, 2006] and the lack of the simulated soil moisture data after 2004.

[36] To illustrate the direct effect of temperature changes, Figure 13a also shows the averaged PDSI time series for the corresponding  $dT = 0$  cases (dashed lines). It can be seen that differences between the all forcing and  $dT = 0$  cases become large since the middle 1980s for all the forms of the PDSI, especially for PDSI\_th and sc\_PDSI\_th (not shown in Figure 13). Without the temperature changes, the recent global drying trends disappear, and the period since the late 1990s becomes wetter than normal for all the forms of the PDSI.

[37] Consistent with Figure 13a, the percentage of the global land areas under drought conditions, defined as the areas within the bottom 20 percentiles of the local PDSI or simulated soil moisture of the analyzed period (e.g., 1950–2008 in Figure 13), exhibits variations and trends opposite to the global-mean PDSI and soil moisture time series. In particular, all the cases in Figure 13b show that the global percentage of dry area stayed around 14%–20% from 1950 to 1982, when it had a sharp jump (by ~10%) during the 1982–1983 El Niño, which reduced precipitation over many land areas [*Dai and Wigley*, 2000]. Since 1983, an upward trend is apparent in all but the PDSI cases without temperature changes (dashed lines), which show little trend from 1983 to 2008. As for the global-mean PDSI series (Figure 13a), the PDSI cases with PE\_th exhibit noticeably larger increases in the percentage dry area than the PDSI cases with PE\_pm and the CLM3 case.

[38] The above results suggest that the use of the Penman-Monteith PE, instead of the Thornthwaite PE, indeed reduces

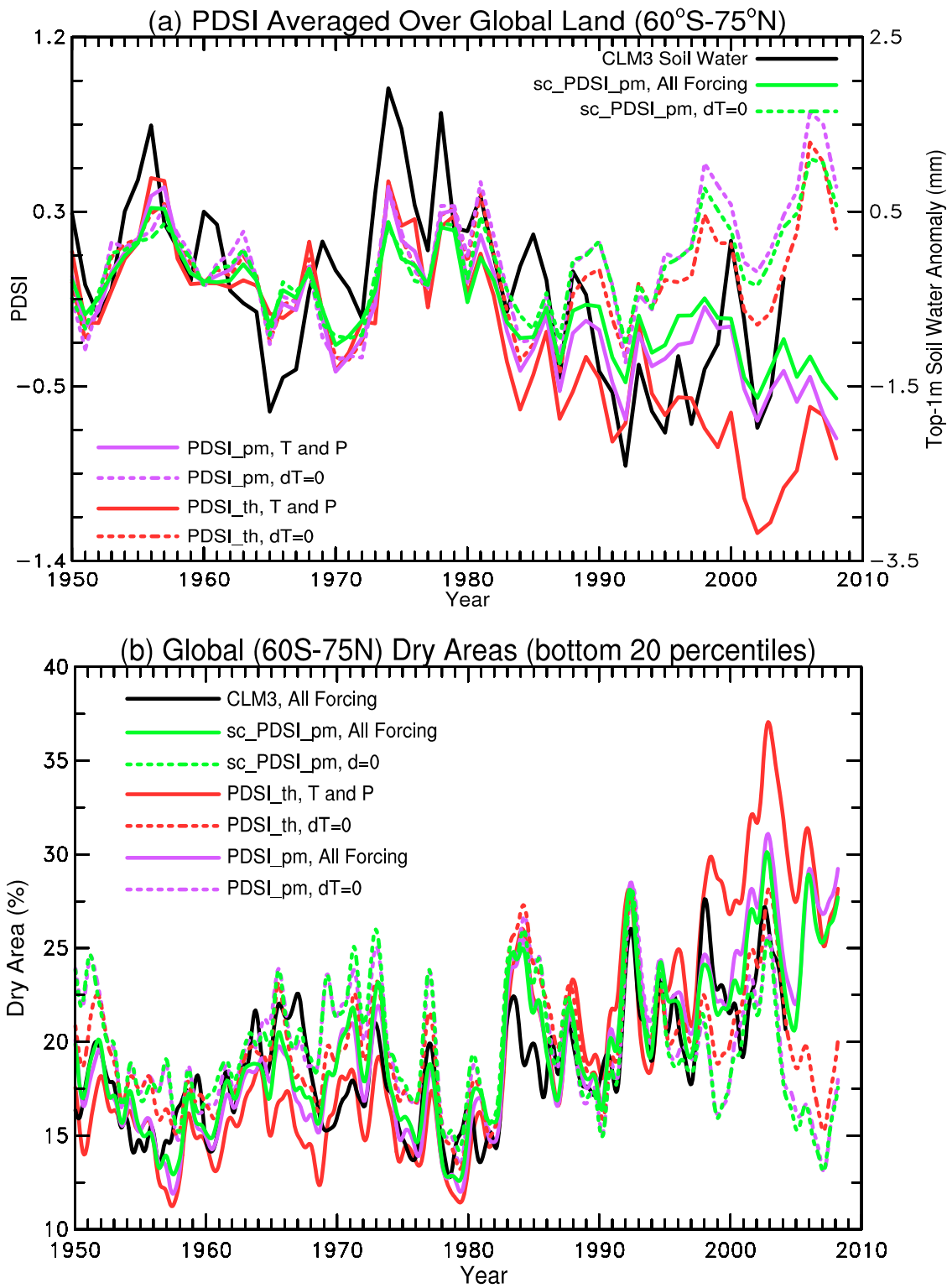


**Figure 13.** (a) Time series of globally ( $60^{\circ}\text{S}$ – $75^{\circ}\text{N}$ ) averaged annual anomalies of PDSI\_th (red), PDSI\_pm (magenta), and sc\_PDSI\_pm (green) computed using all forcing (solid lines) and without temperature changes (dashed lines). Also shown is the global-mean top-1 m soil water content anomaly from a land-model (CLM3) simulation forced with observed precipitation and other historical data [see Qian *et al.*, 2006]. (b) Same as Figure 13a but for smoothed global percentage dry area, defined as the area within the bottom 20 percentiles of the monthly PDSI or CLM3 soil moisture at each grid box. Note that the anomalies in Figure 13a are all relative to the 1950–1977 mean during which global temperature trends are small and thus the differences between the solid and dashed lines are small.

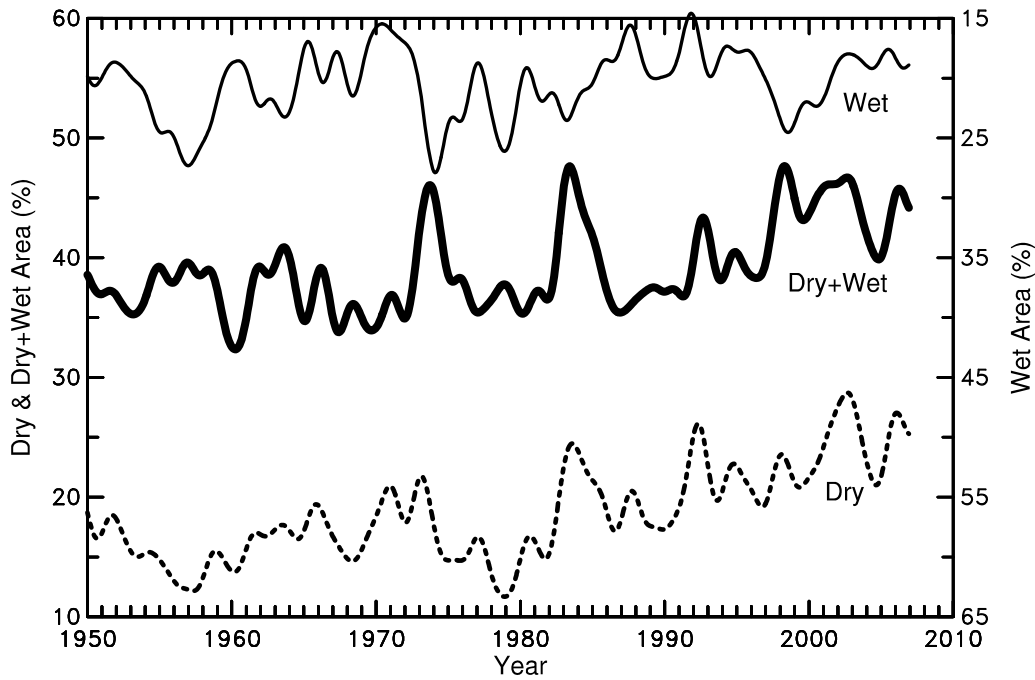


**Figure 14.** Smoothed time series of the percentage dry (dashed line), wet (thin solid line, increases down on the right ordinate), and dry plus wet (thick solid line) areas over the global ( $60^{\circ}\text{S}$ – $75^{\circ}\text{N}$ ) land areas. The dry (wet) areas are defined as the bottom (top) 20 percentiles at each grid box. The sc\_PDSI\_pm was used. Results based on the other forms of the PDSI are similar.

the drying impact of recent warming, resulting in smaller drying trends for the recent decades. This confirms the previous notion that the (original) PDSI may overestimate the drying effect of warming due to its use of the PE\_th [Trenberth *et al.*, 2007, p. 261; Hobbins *et al.*, 2008]. Nevertheless, the PDSI using the Penman-Monteith PE (i.e., PDSI\_pm and sc\_PDSI\_pm) still shows substantial drying during recent decades over many land areas (Figures 11b and 11d) and the global land as a whole (Figure 13). This result is qualitatively

consistent with those of Burke *et al.* [2006] and van der Schrier *et al.* [2011], who also found that the PDSI is not very sensitive to the use of PE\_th or PE\_pm for the 20th century because the CAFEC precipitation (equation (2)) is insensitive to the choice of the PE formulation. Furthermore, this drying is largely due to recent warming, especially since the middle 1980s, as shown by the PDSI and sc\_PDSI values and the percentage of dry areas calculated using the PDSI with either PE\_th or PE\_pm (Figure 13).

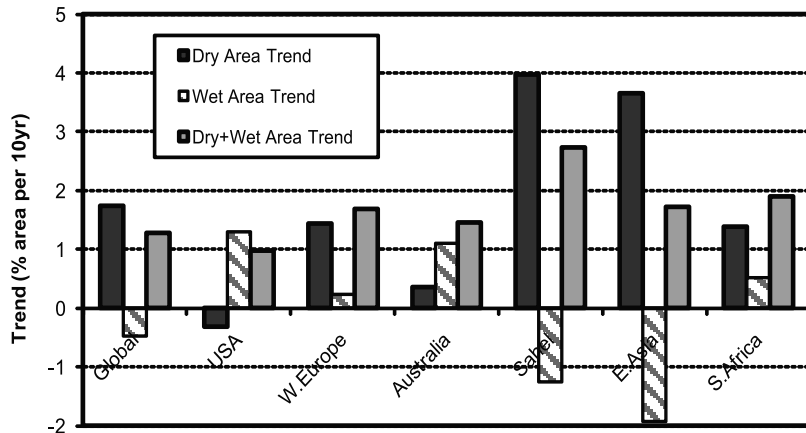


**Figure 15.** Linear trends in the smoothed time series of the percentage dry, wet, and dry plus wet areas shown in Figures 14 and 16. The trends are based the sc\_PDSI\_pm, and they are statistically significant at the 5% level. Results are similar for the other forms of the PDSI, with the drying trend slightly larger when PE\_th is used.

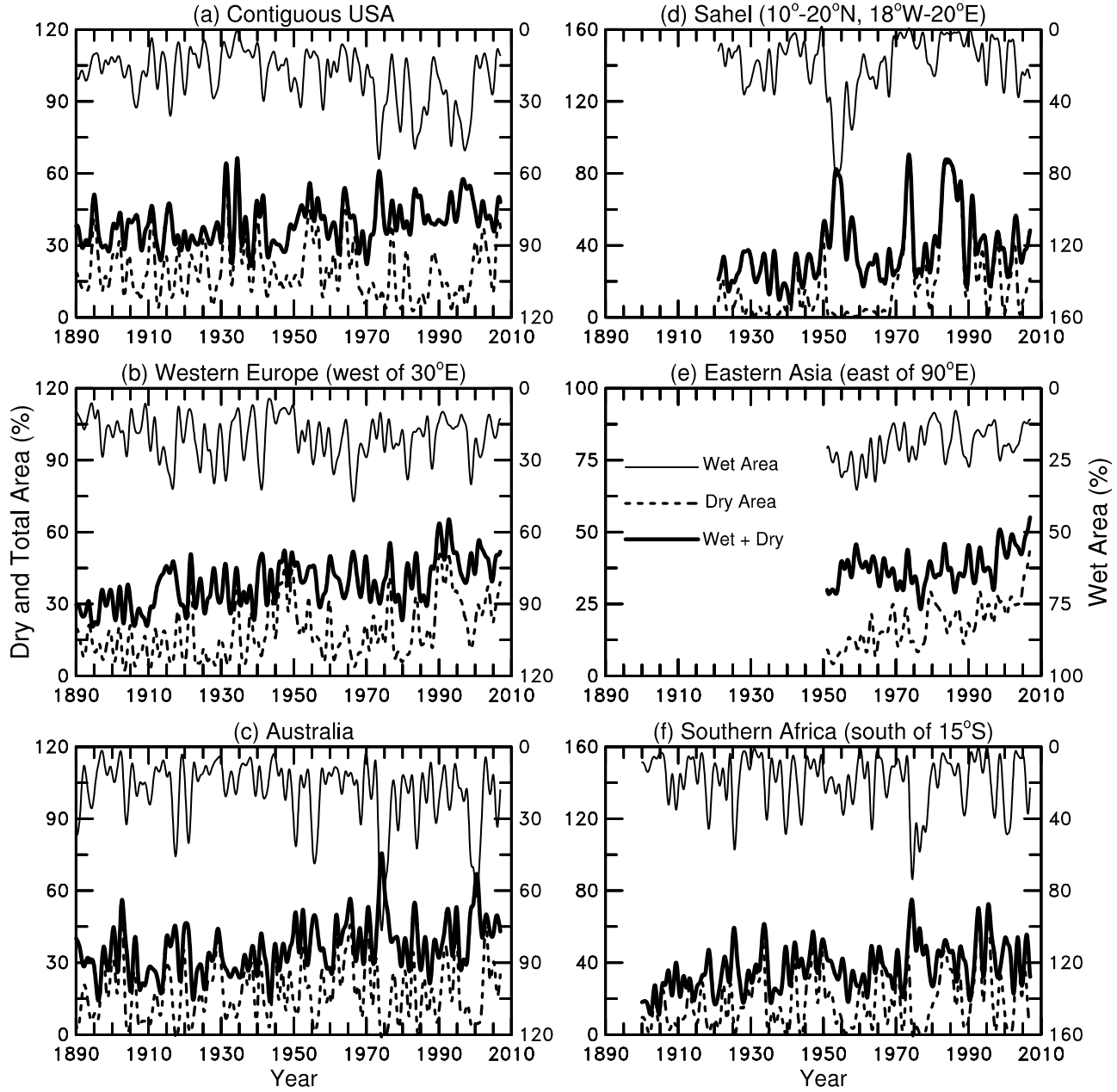


**Figure 16.** Time series of the percentage dry (dashed line), wet (thin solid line), and dry plus wet (thick solid line) areas averaged over six select regions. The dry (wet) areas are defined as the bottom (top) 20 percentiles at each grid box, and the data coverage was required to be 50% or higher in computing the percentages. Note the percentage wet area increases downward on the right ordinate. The sc\_PDSI\_pm was used. Results based the other forms of the PDSI are similar.

[39] Besides the dry spells, areas under wet conditions, defined here as the top 20 percentiles of the PDSI at each grid box, represent the other end of the moisture extremes near the surface. Figure 14 shows that the global percentage wet area varies considerably from ~15% to 26% and often is anticorrelated with the percentage dry area ( $r = -0.45$ ). It contains a small, but still statistically significant, downward trend ( $-0.48\%$  per decade) during 1950–2008 that is not affected greatly by the end points. In contrast, the global percentage dry area shows a much larger upward trend

( $1.74\%$  per decade) during the same period. The global combined areas under either dry or wet conditions show a significant upward trend ( $1.27\%$  per decade) during 1950–2008 (Figures 14 and 15).

### 5.3. Regional Aridity Changes

[40] Figure 16 shows the percentage of dry, wet, and dry plus wet areas for six select regions with relatively good data coverage as far back as 1890, with their linear trends shown in Figure 15. As for the global case shown in Figure 14, the

regional dry and wet areas show large year-to-year variations, and they are often anticorrelated ( $r = -0.5$  to  $-0.7$ ), which reduces the variations in the combined dry plus wet area. In all the regions except the contiguous United States, significant upward trends are seen in both the dry and dry plus wet areas, especially for the Sahel, East Asia, and southern Africa (Figure 15). Over the contiguous United States, precipitation had increased during the later half of the 20th century [Dai, 2011] partly due to a shift to more frequent El Niños since the late 1970s [Trenberth and Hoar, 1997]. This led to an increase in the wet area and a decrease in the dry area from the 1950s to the late 1990s; thereafter, the United States has been experiencing fairly dry conditions with reduced wet areas and increased dry areas (Figure 16a). Despite the negative correlation between the dry and wet areas, some of the regions, such as southern Africa, Australia, and western Europe, show positive trends for both the dry and wet areas, which results in an enhanced upward trend in the combined area under either dry or wet conditions (Figure 15). Other regions (namely the Sahel, East Asia, and the United States) and the global land as whole show opposite trends for the dry and wet areas, and this results in a smaller trend in the combined area (Figure 15). Figure 16 looks similar to Figure 10 of Dai *et al.* [2004], who defined the dry (wet) areas as grid boxes with PDSI\_th less than  $-3.0$  (greater than  $+3.0$ ).

## 6. Summary

[41] To provide a quantitative comparison of the various forms of the PDSI and to update the widely used global PDSI data set created by Dai *et al.* [2004], I have computed monthly values from 1850 to 2008 for four forms of the PDSI over global land areas on a  $2.5^\circ \times 2.5^\circ$  grid (however, many areas do not have data before 1948), made quantitative comparisons among these forms of the PDSI, and evaluated them using available data of soil moisture, streamflow, and water storage from the GRACE satellite over land. Leading modes of variability and long-term changes in the four forms of the PDSI were examined and compared, with a focus on the consistency among the different forms of the PDSI and the impact of the recent warming and the choice of the PE calculations on the PDSI. The main results and conclusions are summarized below. They are generally consistent with previous studies [e.g., Dai *et al.*, 1998, 2004; Burke *et al.*, 2006; van der Schrier *et al.*, 2006a, 2006b, 2011], although many of our results are new or more quantitative, e.g., regarding the differences among the four forms of the PDSI; the correlation with soil moisture, streamflow, and GRACE data; the consistency with CLM3-simulated soil moisture; and the impact of surface warming.

[42] 1. The use of the Penman-Monteith PE, instead of the Thornthwaite PE, in the Palmer model only has small effects on actual evapotranspiration and thus the resultant PDSI, and it only slightly reduces the widespread drying represented by the PDSI during recent decades over global land. This result confirms the finding of van der Schrier *et al.* [2011], who found that the sc\_PDSI does not change a lot when either PE\_th or PE\_pm was used because of the insensitivity of the CAFEC precipitation (equation (2)) to PE. I realize that large uncertainties exist in historical data for surface net radiation, wind speed, and humidity needed for computing the Penman-Monteith PE, and further work is needed to improve the

quality of these forcing data. However, it is unlikely that large long-term trends in these three variables have occurred since 1950 but are not reflected in our forcing data, partly because our use of observed cloudiness changes. The small difference between the PDSI using PE\_th and PE\_pm suggests that the effects on the PDSI from long-term changes in surface net radiation, wind speed, and humidity are likely small since 1950.

[43] 2. The self-calibration proposed by Wells *et al.* [2004] for the sc\_PDSI indeed reduces the PDSI range over many land areas and improves its spatial comparability and the symmetry of its histograms. However, the monthly sc\_PDSI still has a non-Gaussian distribution at many locations.

[44] 3. All four forms of the PDSI, namely, PDSI\_th, PDSI\_pm, sc\_PDSI\_th, and sc\_PDSI\_pm, are significantly correlated with observed soil moisture ( $r = 0.4\text{--}0.8$ ) over a number of regions in the United States and Eurasia, and basin-averaged yearly PDSI values during 1948–2004 are correlated ( $r = 0.4\text{--}0.9$ ) with observed yearly streamflow for 87% of the world's largest 230 river basins for which I had data. The correlation with the land water storage from GRACE during 2002–2008 is also similar among the different forms of the PDSI, with an  $r = 0.4\text{--}0.8$  over most land areas. These correlations exist even over many high-latitude cold regions, suggesting that the PDSI can be used to depict yearly aridity changes even at high latitudes. However, it should be noticed that the evaluation done here using historical records may not be applicable for future climates, where the impacts of rapidly rising temperatures and downward longwave radiation become increasingly important.

[45] 4. Similar to the leading EOF modes in the original PDSI using the Thornthwaite PE (i.e., PDSI\_th [see Dai *et al.*, 2004; Dai, 2011]), the first leading mode in the other forms of the PDSI also depicts a long-term trend since around 1950 of drying over most of Africa, East and South Asia, the Mediterranean region, eastern Australia, and midlatitude Canada and wetting over the contiguous United States, Argentina, western Australia, and parts of central and northern Eurasia; the second mode is associated with ENSO, with drying during El Niños over the South Asia-Australia region, southern Africa, and northern South America and wetting over the southwestern U.S.-Mexican region, Argentina, East Africa, and central Eurasia.

[46] 5. All four forms of the PDSI show widespread drying over Africa, East and South Asia, and other areas from 1950 to 2008, and most of this drying is due to recent warming. The global dry areas have increased by about 1.74% (of global land area) per decade from 1950 to 2008. The use of the Penman-Monteith PE and self-calibrating PDSI only slightly reduces the drying trend seen in the original PDSI.

[47] 6. The percentages of dry and wet areas over the global land area and six select regions are anticorrelated ( $r = -0.5$  to  $-0.7$ ), but their long-term trends do not cancel each other. The trend for the dry area often predominates over that for the wet area, which results in upward trends for the combined dry and wet areas. In other words, areas under extreme (i.e., dry or wet) conditions have increased since 1950 by  $\sim 1.27\%$  per decade for the global land as a whole, and over all the six regions examined (Figure 15).

[48] The recent widespread drying trend and the effect of surface warming are qualitatively consistent with the observed decreases in streamflow over many low and midlatitude river

basins [Dai *et al.*, 2009]. Our PDSI trends are broadly comparable with those in the soil moisture simulated by another land surface model [Sheffield and Wood, 2008a]. The results are also consistent with the model-predicted 21st century climate, which shows severe drought conditions by the middle of this century over most low and midlatitude land areas [Wang, 2005; Sheffield and Wood, 2008b; Dai, 2011]. Thus, I believe that our main conclusion is robust that recent warming has caused widespread drying over land. And model predictions suggest that this drying is likely to become more severe in the coming decades [Dai, 2011].

## Appendix A: Duration and Scaling Factors for Self-Calibrated PDSI

[49] As mentioned in section 3.1, Wells *et al.* [2004] described the procedures to estimate the duration factors  $p$  and  $q$  but did not discuss the details regarding how one should define the most extreme droughts for estimating the  $p$  and  $q$ . Here I discuss the results from our tests using slightly different methods in estimating these factors. I also present the global maps for the  $K$  scaling factor, namely,  $K_o$  in equation (3).

[50] I tested various lengths for the regression between the length and (cumulative) severity of the most extreme drought (Figure A1). I found that, for many locations, consecutive dry spells usually do not last longer than about 18 months over our calibration period (1950–1979; results were similar when

$$PE\_th = \begin{cases} 0 \\ 25.4d_u \exp[-3.863233 + 1.715598B - B \ln(H) - B_u \ln(T - 32)] \\ 25.4d_u[\sin(T/57.3 - 0.166) - 0.76] \end{cases}$$

1950–1999 was used) and the slopes do not change a lot beyond this length (Figure A1). Thus, I used the length of 18 months in the regression for estimating the duration factors  $p$  and  $q$ . I also tested three slightly different methods in defining the driest and wettest spells (i.e., the sum of the  $Z$  index in Figure A1). Method 1 uses all the  $Z$  values in the summation and finds the smallest sum as the  $Z$ -sum value for the driest spell and the largest sum as the  $Z$ -sum value for the wettest spell for a given time length (Figures A1a and A1b). Method 2 uses only the negative (positive)  $Z$  values for the summation for dry (wet) spells, while method 3 uses only the consecutive negative (positive)  $Z$  values in the summation for dry (wet) spells. As a result, method 3 yields few spells exceeding 18 months (Figures A1c and A1f).

[51] Figures A2a–A2f show that the spatial distributions of the  $p$  and  $q$  values for dry cases are similar using methods 1 and 2. For method 3, the  $p$  ( $q$ ) values are slightly lower (higher) than those from methods 1 and 2. Although our  $p$  and  $q$  values do not differ greatly from Palmer's original estimates of  $p = 0.897$  and  $q = 1/3$  using limited data from Kansas and Iowa, there are considerable spatial variations. In particular, the  $q$  values for the deserts in northern Africa, central Asia, and southwestern Australia are relatively large due to the lack of variability in these regions that leads to small  $Z$  variations and thus small sum of the  $Z$  index (see Figure A1).

[52] Palmer [1965] used the same duration factors in equation (4) for both dry and wet spells. For the sc\_PDSI, Wells *et al.* [2004] used separate duration factors for the dry and wet cases computed based on the slopes for the dry

and wet cases shown in Figure A1. For the wet cases, the differences and similarity of the duration factors among methods 1–3 are comparable to those for the dry cases shown in Figures A2a–A2f. Thus, I only show the  $p$  and  $q$  maps from method 2 for the wet cases in Figures A2g and A2h. It can be seen that the  $p$  ( $q$ ) values are somewhat larger (smaller) than those for the dry cases. The sc\_PDSI values computed using methods 1–3 differ only slightly. In this paper, I only show results using method 2.

[53] For the original PDSI, the climatic characteristic  $K$  is computed using the  $K_o$  given in equation (3), whose spatial distribution is shown in Figure A3a. This  $K_o$  is generally larger at northern mid-high latitudes and in northern Africa than in other regions. For the sc\_PDSI,  $K_o$  is defined as  $-4/(\text{the second percentile of the PDSI})$  for the dry cases and as  $+4/(\text{the 98th percentile of the PDSI})$  for the wet cases (see equation (9) from Wells *et al.* [2004]). For comparison, these  $K_o$  values are shown in Figures A3b and A3c. They are much more homogeneous spatially and comparable to Palmer's  $K_o$  values over the Midwest United States.

## Appendix B: Calculations of PE

[54] Palmer [1965] used the Thornthwaite [1948] equation to compute the PE as a function of monthly mean surface air temperature, latitude, and month. I used the following implementation of the Thornthwaite PE ( $PE\_th$ , in mm/day) adapted from the National Climatic Data Center [Karl, 1986]:

$$PE\_th = \begin{cases} \ln(H) - B_u \ln(T - 32) & \text{for } 32^\circ F < T < 80^\circ F, \\ \text{for } T \geq 80^\circ F \end{cases} \quad (B1)$$

where  $T$  is monthly mean surface air temperature in  $^\circ F$  ( $= 32 + 9/5 t$ , where  $t$  is in  $^\circ C$ ),  $\theta$  is the latitude, and  $\phi(m)$  is a month ( $m$ )-dependent coefficient.  $B$  and  $H$  are two heat factors calculated as follows.

$$H = \sum_{m=1}^{12} \left( \frac{\max(t, 0)}{5} \right)^{1.514}, \quad (B2)$$

$$B = 0.492 + 1.79 \times 10^{-2}H - 7.71 \times 10^{-5}H^2 + 6.75 \times 10^{-7}H^3. \quad (B3)$$

And  $d_u$  in (B1) is defined as

$$d_u = \begin{cases} (d_o + 0.0157)/1.57 & \text{if } d_o \geq 0 \\ [(3.141593 + d_o) + 0.0157]/1.57 & \text{if } d_o < 0 \end{cases}$$

$$\text{where } d_o = \tan^{-1} \left( \frac{\sqrt{\max(0.1, 1 - [\phi(m) \tan(\theta)]^2)}}{-\phi(m) \tan(\theta)} \right). \quad (B4)$$

A more physically based and widely used formula for computing PE is the Penman-Monteith equation. Here I used the version recommended by Shuttleworth [1993].

$$PE\_pm = \frac{\Delta}{\Delta + \gamma} (R_n + A_h) + \frac{\Delta}{\Delta + \gamma} \frac{6.43(1 + 0.536U_2)D}{\lambda}, \quad (B5)$$

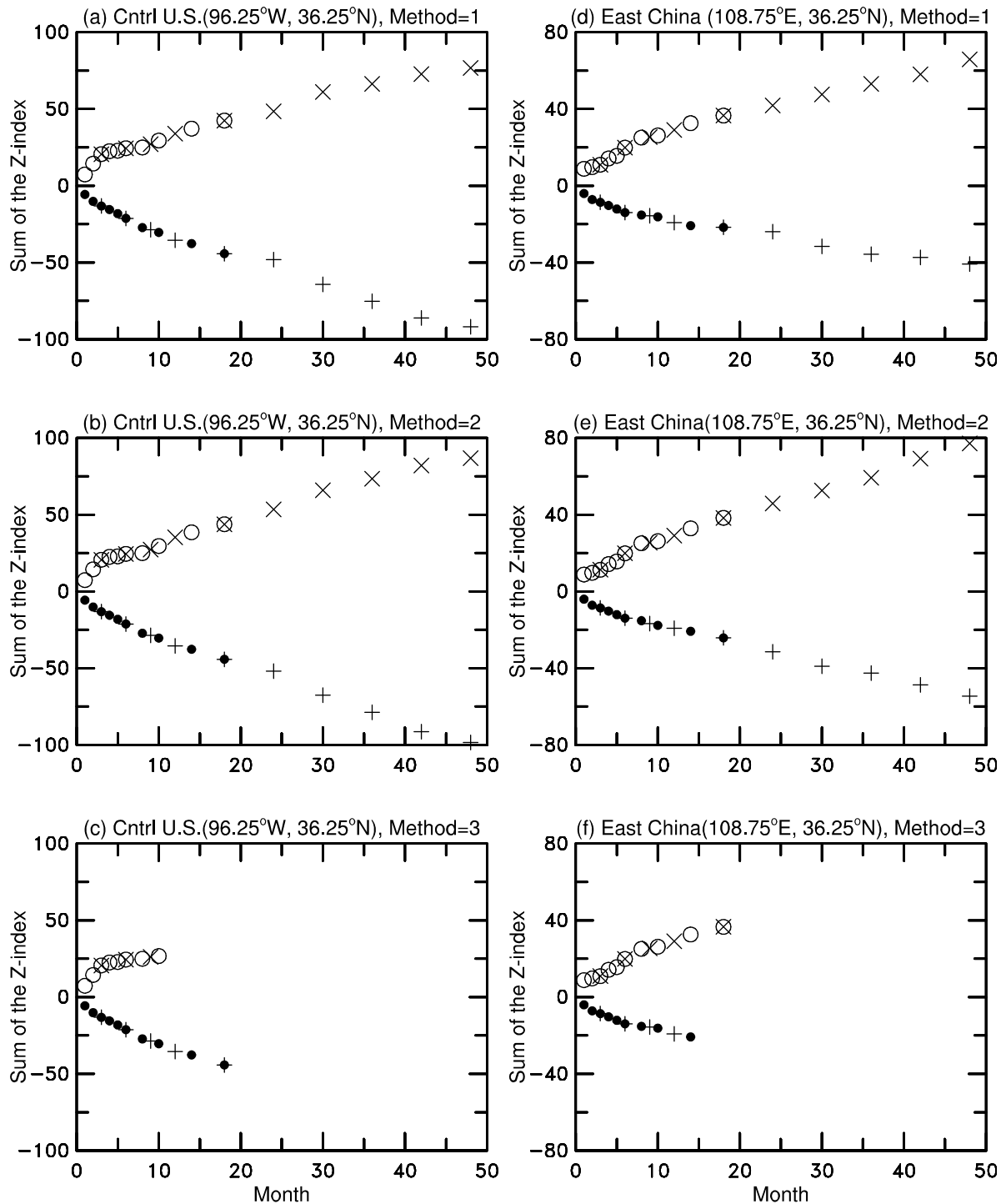


**Figure A1.** The accumulated Z index over the driest (solid circle and plus) and wettest (open circle and cross) intervals of varying lengths at a grid box in (a, b, c) the central United States and (d, e, f) East China computed using three slightly different methods (see Appendix A for details).

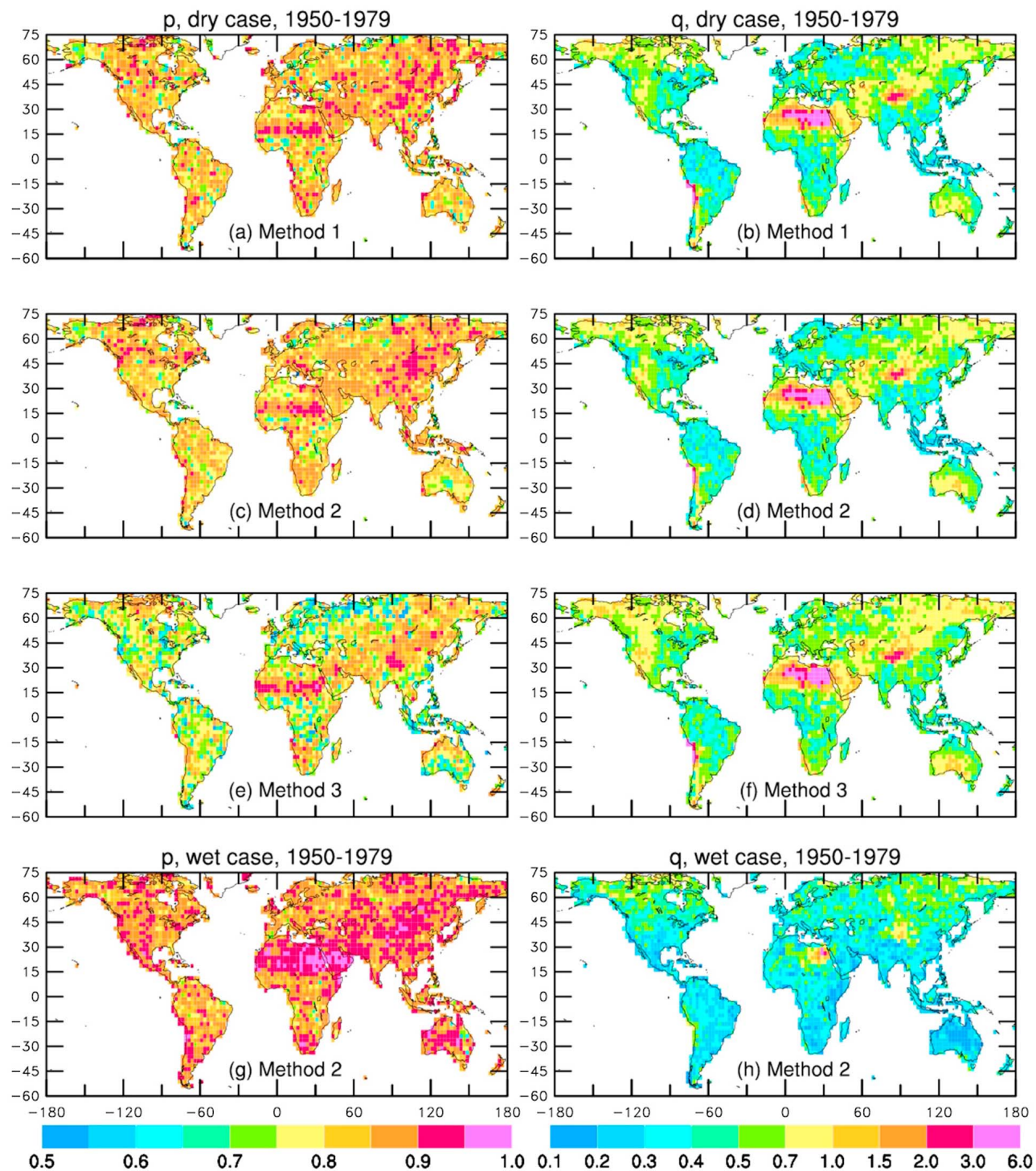


**Figure A2.** The (a, c, e, g)  $p$  and (b, d, f, h)  $q$  parameters used in the sc\_PDSI calculations for (a-f) dry cases using three slightly different methods (Figures A2a-A2f) and for wet cases using method 2 (Figures A2g and A2h). The PE\_pm was used in the calculations (similar if PE\_th was used).

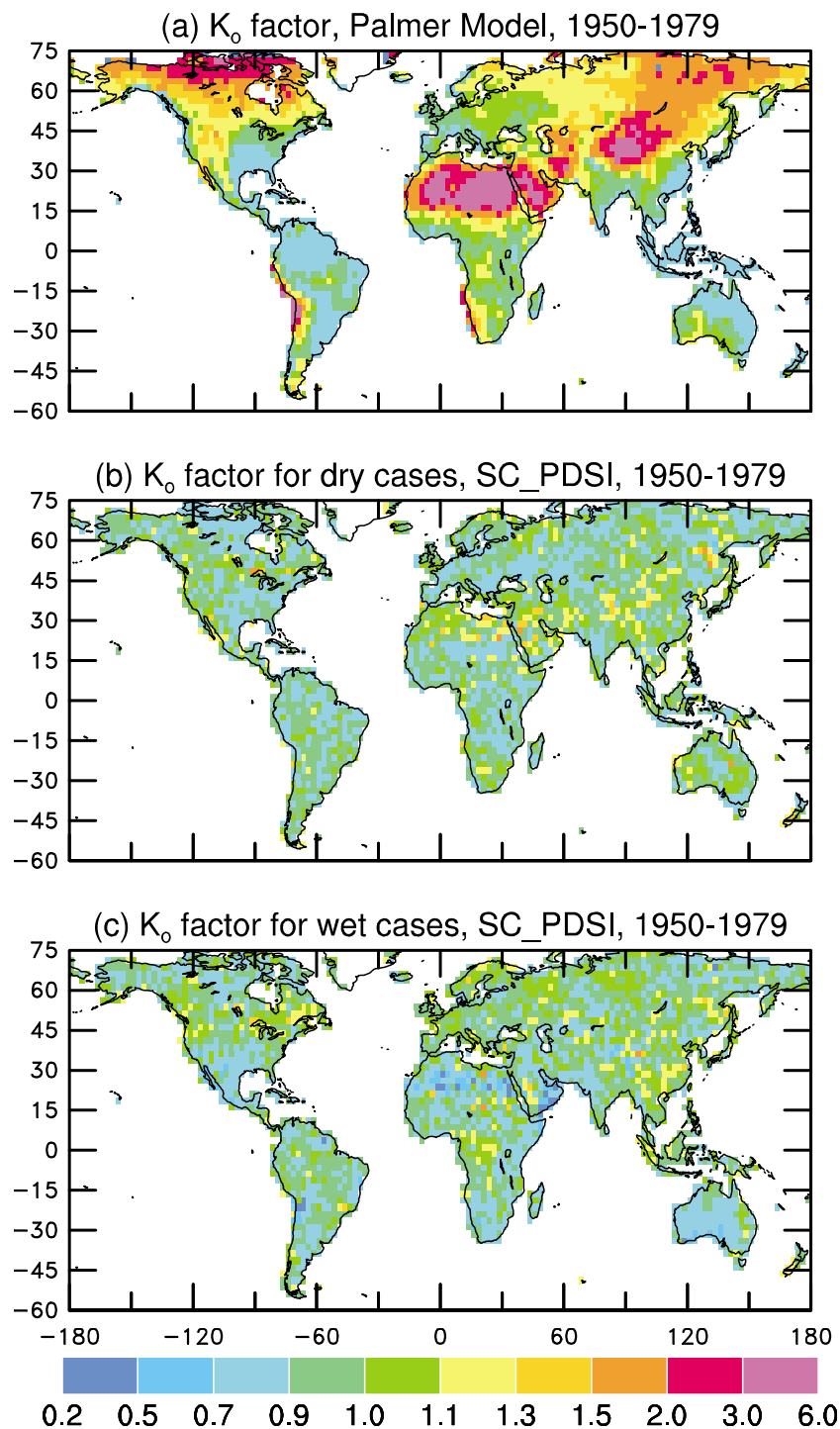


**Figure A3.** The  $K_o$  scaling factor for (a) both the wet and dry cases in the original Palmer model and for the (b) dry and (c) wet cases for the sc\_PDSI. Data for 1950–1979 and the Penman-Monteith PE were used in this calculation.

where  $R_n$  is the net surface radiation, converted to  $\text{mm day}^{-1}$ ,  $A_h$  is the surface horizontal energy convergence (ignored here),  $U_2$  is surface (2 m) wind speed in  $\text{m s}^{-1}$ , and  $D$  is surface vapor pressure deficit in kPa. The coefficients  $\Delta$ ,  $\gamma$ , and  $\lambda$  are given by Shuttleworth [1993]. Thus,  $PE_{pm}$  increases with surface net radiation, wind speed, and vapor pressure deficit. The Penman-Monteith PE has been shown to perform better than other formulations over Australia [Donohue *et al.*, 2010].

[55] **Acknowledgments.** I thank G. van der Schrier, Phil Jones, and Chris Milly for constructive discussions and acknowledge the support from the NCAR Water Systems Program. The GRACE land data were processed by Sean Swenson, supported by the NASA MEASURES Program, and are available at <http://grace.jpl.nasa.gov>. The PDSI data will be freely available from <http://www.cgd.ucar.edu/cas/catalog/climind/pdsi.html>. The National Center for Atmospheric Research is sponsored by the U.S. National Science Foundation.

## References

- Alley, W. M. (1984), Palmer drought severity index: Limitations and assumptions, *J. Clim. Appl. Meteorol.*, **23**, 1100–1109, doi:10.1175/1520-0450(1984)023<1100:TPDSIL>2.0.CO;2.
- Brohan, P., J. J. Kennedy, I. Harris, S. F. B. Tett, and P. D. Jones (2006), Uncertainty estimates in regional and global observed temperature changes: A new dataset from 1850, *J. Geophys. Res.*, **111**, D12106, doi:10.1029/2005JD006548.
- Brutsaert, W. (2006), Indications of increasing land surface evaporation during the second half of the 20th century, *Geophys. Res. Lett.*, **33**, L20403, doi:10.1029/2006GL027532.
- Burke, E. J., and S. J. Brown (2008), Evaluating uncertainties in the projection of future drought, *J. Hydrometeorol.*, **9**, 292–299, doi:10.1175/2007JHM929.1.
- Burke, E. J., S. J. Brown, and N. Christidis (2006), Modeling the recent evolution of global drought and projections for the twenty-first century with the Hadley Centre climate model, *J. Hydrometeorol.*, **7**, 1113–1125, doi:10.1175/JHM544.1.
- Chen, M., P. Xie, J. E. Janowiak, and P. A. Arkin (2002), Global land precipitation: A 50-yr monthly analysis based on gauge observations, *J. Hydrometeorol.*, **3**, 249–266, doi:10.1175/1525-7541(2002)003<0249:GLPAYM>2.0.CO;2.
- Cook, E. R., C. A. Woodhouse, C. M. Eakin, D. M. Meko, and D. W. Stahle (2004), Long-term aridity changes in the western United States, *Science*, **306**, 1015–1018, doi:10.1126/science.1102586.
- Cook, E. R., R. Seager, M. A. Cane, and D. W. Stahle (2007), North American drought: Reconstructions, causes, and consequences, *Earth Sci. Rev.*, **81**, 93–134, doi:10.1016/j.earscirev.2006.12.002.
- Dai, A. (2006), Recent climatology, variability and trends in global surface humidity, *J. Clim.*, **19**, 3589–3606, doi:10.1175/JCLI3816.1.
- Dai, A. (2011), Drought under global warming: A review, *WIREs Clim. Change*, **2**, 45–65, doi:10.1002/wcc.81.
- Dai, A. G., and T. M. L. Wigley (2000), Global patterns of ENSO-induced precipitation, *Geophys. Res. Lett.*, **27**, 1283–1286, doi:10.1029/1999GL011140.
- Dai, A., I. Y. Fung, and A. D. Del Genio (1997), Surface observed global land precipitation variations during 1900–88, *J. Clim.*, **10**, 2943–2962, doi:10.1175/1520-0442(1997)010<2943:SOGLPV>2.0.CO;2.
- Dai, A., K. E. Trenberth, and T. R. Karl (1998), Global variations in droughts and wet spells: 1900–1995, *Geophys. Res. Lett.*, **25**, 3367–3370, doi:10.1029/98GL52511.
- Dai, A., K. E. Trenberth, and T. T. Qian (2004), A global dataset of Palmer Drought Severity Index for 1870–2002: Relationship with soil moisture and effects of surface warming, *J. Hydrometeorol.*, **5**, 1117–1130, doi:10.1175/JHM-386.1.
- Dai, A., T. R. Karl, B. Sun, and K. E. Trenberth (2006), Recent trends in cloudiness over the United States: A tale of monitoring inadequacies, *Bull. Am. Meteorol. Soc.*, **87**, 597–606, doi:10.1175/BAMS-87-5-597.
- Dai, A. G., T. T. Qian, K. E. Trenberth, and J. D. Milliman (2009), Changes in continental freshwater discharge from 1948 to 2004, *J. Clim.*, **22**, 2773–2792, doi:10.1175/2008JCLI2592.1.
- Donohue, R. J., T. R. McVicar, and M. L. Roderick (2010), Assessing the ability of potential evaporation formulations to capture the dynamics in evaporative demand within a changing climate, *J. Hydrol.*, **386**, 186–197, doi:10.1016/j.jhydrol.2010.03.020.
- Guttman, N. B., J. R. Wallis, and J. R. M. Hosking (1992), Spatial comparability of the Palmer Drought Severity Index, *Water Resour. Bull.*, **28**, 1111–1119.
- Heim, R. R., Jr. (2000), Drought indices: A review, in *Drought: A Global Assessment*, edited by D. A. Wilhite, pp. 159–167, Routledge, London.
- Heim, R. R., Jr. (2002), A review of twentieth-century drought indices used in the United States, *Bull. Am. Meteorol. Soc.*, **83**, 1149–1165.
- Hobbins, M. T., A. Dai, M. L. Roderick, and G. D. Farquhar (2008), Revisiting potential evapotranspiration parameterizations as drivers of long-term water balance trends, *Geophys. Res. Lett.*, **35**, L12403, doi:10.1029/2008GL033840.
- Hollinger, S. E., and S. A. Isard (1994), A soil-moisture climatology of Illinois, *J. Clim.*, **7**, 822–833, doi:10.1175/1520-0442(1994)007<0822:ASMCOI>2.0.CO;2.
- Huffman, G. J., R. F. Adler, D. T. Bolvin, and G. J. Gu (2009), Improving the global precipitation record: GPCC version 2.1, *Geophys. Res. Lett.*, **36**, L17808, doi:10.1029/2009GL040000.
- Kalnay, E., et al. (1996), The NCEP/NCAR 40-year reanalysis project, *Bull. Am. Meteorol. Soc.*, **77**, 437–471, doi:10.1175/1520-0477(1996)077<0437:TNYRP>2.0.CO;2.
- Karl, T. R. (1986), Sensitivity of the Palmer drought severity index and Palmer's Z-index to their calibration coefficients including potential evapotranspiration, *J. Clim. Appl. Meteorol.*, **25**, 77–86, doi:10.1175/1520-0450(1986)025<0077:TSOTPD>2.0.CO;2.
- Keyantash, J., and J. A. Dracup (2002), The quantification of drought: An evaluation of drought indices, *Bull. Am. Meteorol. Soc.*, **83**, 1167–1180.
- Milliman, J. D., K. L. Farnsworth, P. D. Jones, K. H. Xu, and L. C. Smith (2008), Climatic and anthropogenic factors affecting river discharge to the global ocean, 1951–2000, *Global Planet. Change*, **62**, 187–194, doi:10.1016/j.gloplacha.2008.03.001.
- Mitchell, T. D., and P. D. Jones (2005), An improved method of constructing a database of monthly climate observations and associated high-resolution grids, *Int. J. Climatol.*, **25**, 693–712, doi:10.1002/joc.1181.
- Palmer, W. C. (1965), Meteorological drought, *Rep.*, **45**, 58 pp., U.S. Dept. of Commerce, Washington, D. C. (Available at <http://www.ncdc.noaa.gov/oa/climate/research/drought/palmer.pdf>).
- Qian, T., A. Dai, K. E. Trenberth, and K. W. Oleson (2006), Simulation of global land surface conditions from 1948–2004. Part I: Forcing data and evaluation, *J. Hydrometeorol.*, **7**, 953–975, doi:10.1175/JHM540.1.
- Robock, A., K. Y. Vinnikov, G. Srinivasan, J. K. Entin, S. E. Hollinger, N. A. Speranskaya, S. Liu, and A. Namkhai (2000), The Global Soil Moisture Data Bank, *Bull. Am. Meteorol. Soc.*, **81**, 1281–1299.
- Roderick, M. L., L. D. Rotstayn, G. D. Farquhar, and M. T. Hobbins (2007), On the attribution of changing pan evaporation, *Geophys. Res. Lett.*, **34**, L17403, doi:10.1029/2007GL031166.
- Sheffield, J., and E. F. Wood (2008a), Global trends and variability in soil moisture and drought characteristics, 1950–2000, from observation-driven simulations of the terrestrial hydrologic cycle, *J. Clim.*, **21**, 432–458, doi:10.1175/2007JCLI1822.1.
- Sheffield, J., and E. F. Wood (2008b), Projected changes in drought occurrence under future global warming from multi-model, multi-scenario, IPCC AR4 simulations, *Clim. Dyn.*, **31**, 79–105, doi:10.1007/s00382-007-0340-z.
- Shuttleworth, W. J. (1993), Evaporation, in *Handbook of Hydrology*, edited by D. R. Maidment, pp. 4.1–4.53, McGraw-Hill, New York.
- Swenson, S. C., and J. Wahr (2006), Post-processing removal of correlated errors in GRACE data, *Geophys. Res. Lett.*, **33**, L08402, doi:10.1029/2005GL025285.
- Swenson, S., P. J. F. Yeh, J. Wahr, and J. Famiglietti (2006), A comparison of terrestrial water storage variations from GRACE with in situ measurements from Illinois, *Geophys. Res. Lett.*, **33**, L16401, doi:10.1029/2006GL026962.
- Thornthwaite, C. W. (1948), An approach toward a rational classification of climate, *Geogr. Rev.*, **38**, 55–94, doi:10.2307/210739.
- Trenberth, K. E., and T. J. Hoar (1997), El Niño and climate change, *Geophys. Res. Lett.*, **24**, 3057–3060, doi:10.1029/97GL03092.
- Trenberth, K. E., et al. (2007), Observations: Surface and atmospheric climate change, in *Climate Change 2007: The Physical Science Basis*, edited by S. Solomon et al., pp. 235–336, Cambridge Univ. Press, Cambridge, U. K.
- van der Schrier, G., K. R. Briffa, P. D. Jones, and T. J. Osborn (2006a), Summer moisture variability across Europe, *J. Clim.*, **19**, 2818–2834, doi:10.1175/JCLI3734.1.
- van der Schrier, G., K. R. Briffa, T. J. Osborn, and E. R. Cook (2006b), Summer moisture availability across North America, *J. Geophys. Res.*, **111**, D11102, doi:10.1029/2005JD006745.
- van der Schrier, G., D. Efthymiadis, K. R. Briffa, and P. D. Jones (2007), European Alpine moisture variability for 1800–2003, *Int. J. Climatol.*, **27**, 415–427, doi:10.1002/joc.1411.
- van der Schrier, G., P. D. Jones, and K. R. Briffa (2011), The sensitivity of the PDSI to the Thornthwaite and Penman-Monteith parameterizations for the potential evapotranspiration, *J. Geophys. Res.*, **116**, D03106, doi:10.1029/2010JD015001.

- Vicente-Serrano, S. M., S. Begueria, and J. I. Lopez-Moreno (2010a), A multiscalar drought index sensitive to global warming: The standardized precipitation evapotranspiration index, *J. Clim.*, *23*, 1696–1718, doi:10.1175/2009JCLI2909.1.
- Vicente-Serrano, S. M., S. Begueria, J. I. Lopez-Moreno, M. Angulo, and A. El Kenawy (2010b), A new global 0.5 degrees gridded dataset (1901–2006) of a multiscalar drought index: Comparison with current drought index datasets based on the Palmer Drought Severity Index, *J. Hydrometeorol.*, *11*, 1033–1043, doi:10.1175/2010JHM1224.1.
- Vinnikov, K., and I. B. Yeserkepova (1991), Soil moisture: Empirical data and model results, *J. Clim.*, *4*, 66–79, doi:10.1175/1520-0442(1991)004<0066:SMEDAM>2.0.CO;2.
- Wang, G. L. (2005), Agricultural drought in a future climate: Results from 15 global climate models participating in the IPCC 4th assessment, *Clim. Dyn.*, *25*, 739–753, doi:10.1007/s00382-005-0057-9.
- Webb, R. S., C. E. Rosenzweig, and E. R. Levine (1993), Specifying land surface characteristics in general circulation models: Soil profile data set and derived water-holding capacities, *Global Biogeochem. Cycles*, *7*, 97–108, doi:10.1029/92GB01822.
- Wells, N., S. Goddard, and M. J. Hayes (2004), A self-calibrating Palmer Drought Severity Index, *J. Clim.*, *17*, 2335–2351, doi:10.1175/1520-0442(2004)017<2335:ASPDSI>2.0.CO;2.
- Wilhite, D. A. (2000), Drought as a natural hazard: Concepts and definitions, in *Droughts: A Global Assessment*, edited by D. A. Wilhite, pp. 3–18, Routledge, London.
- Willmott, C. J., C. M. Rowe, and Y. Mintz (1985), Climatology of the terrestrial seasonal water cycle, *J. Climatol.*, *5*, 589–606.

---

A. Dai, National Center for Atmospheric Research, PO Box 3000, Boulder, CO 80307-3000, USA. (adai@ucar.edu)